Quantum Dynamics in Dissipative Environments

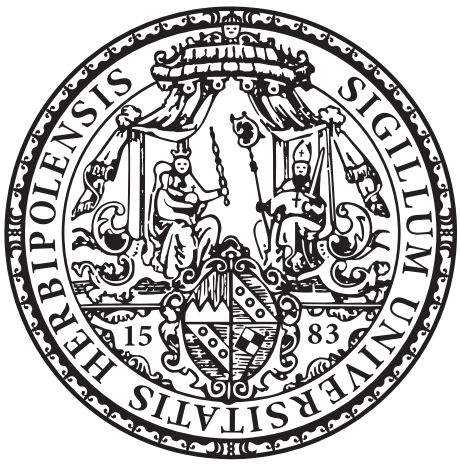

Dissertation

zur Erlangung des naturwissenschaftlichen Doktorgrades
der Julius-Maximilians-Universität Würzburg
vorgelegt von

Robert Kritzer

aus Hamburg

Würzburg 2012

Eingereicht am: .....

bei der Fakultät für Chemie und Pharmazie.

1. Gutachter: .....

2. Gutachter: .....

der Dissertation.

1. Prüfer .....

2. Prüfer .....

3. Prüfer .....

im Promotionskolloquium

Tag des Promotionskolloquiums: .....

Doktorurkunde ausgehändigt am: .....

„Kann mir jemand überzeugend dartun, dass ich nicht richtig urteile oder verfahre, so will ich's mit Freuden anders machen. Suche ich ja nur die Wahrheit, sie, von der niemand je Schaden erlitten hat. Wohl aber erleidet derjenige Schaden, der auf seinem Irrtum und auf seiner Unwissenheit beharrt."

Marc Aurel, Selbstbetrachtungen 6,21

Contents

1. Introduction

The control of molecular chemical reactions using coherent light sources and the prediction of their outcome is a main goal of modern physical chemistry. The present theoretical treatment of control processes under the dissipative influence of an environment aims at a deeper understanding of the feasibility of quantum control.

A variety of control schemes has been developed which are summarised in the monographs by Rice and Zhao [RZ00] and Brumer and Shapiro [BS03b]. In the mid-eighties [BS86] the latter authors suggested to use low intensity coherent light in order to selectively control chemical reactions in the frequency domain. They introduced an active control method to achieve desired product ratios in unimolecular reactions via interference effects induced by phase-varied laser pulses. Tannor et al. [TKR86] developed a pump-dump scheme in time-domain, in which resonant multiphoton processes between different molecular electronic states are utilised to access specific reaction channels. There, an ultrashort laser pulse generates time-dependent wave packets propagating in an excited state. By controlling the delay between pump- and dump-pulse the propagation at different stages is used to generate different outcomes.

Another way to optimise control processes was proposed by Peirce et al. [PDR88], which is based on iterative variational algorithms. This so called Optimal Control Theory relies on successive solutions of the time-dependent Schrödinger equation which yields an optimal field inducing transitions from an initial to a defined target state. A more recent overview on coherent control of molecular dynamics was published in 2003 [BS03a].

In the mentioned approaches the fields are constructed globally in time, i.e., they are obtained incorporating the dynamics over the entire time interval of interest. Alternatively, a local control scheme was introduced by Kosloff et al. [KRG+89]. There, the laser pulse is determined from the instantaneous response of the perturbed system so that, at every point in time, the system dynamics effects the control field generation. In an interesting application of local control theory, Malinovsky et al. [MMT97] demonstrated the so called "optical paralysis" in a large-amplitude vibrational motion. Despite the fact that a strong field excites higher unwanted levels, their population can be kept locked by this procedure only varying the field's phase.

Earlier studies in our group [GME05] investigated the efficiency of local control processes like energetic heating and cooling of a system, selective mode excitation, control of branching ratios in dissociation or electronic population transfer [GEE05]. The temporal evolution of an observable is regulated and the favoured control target is reached, for a recent review see Ref. [EMT09]. Nonetheless, simulations rest on an isolated system perturbed only by the control field as commonly realised in molecular beam experiments [Pau00].

Zewail [ZBD89] was rewarded with the Nobel Prize in 1999 for his work in femtochemistry. This time regime of molecular vibrations is accessible in experiments with lasers only three decades after the first one was built [Mai60].

Engineering concepts in photochemistry are summarised in Warren et al. [WRD93]. The use of pulse shapers, starting with Heritage et al. [HWT85] and Nelson et al. [NRD94], enlarges the experimental possibilities for laser control and peaks in techniques applicable to femtosecond pulses [Wei00] at the turn of the millennium. By now, coherent light source properties as amplitude, phase and polarisation can be affected to generate desired fields to effect molecular motion.

The first control experiments using an adaptive approach were performed by Assion et al. [ABB+98]. Computer learning algorithms, based on an evolution strategy approach, iteratively improve the applied laser pulses by monitoring the yield. In this way the shape of the input fields are modified, via blocking dispersed frequencies by a liquid crystal display until an optimal outcome is reached. Brixner et al. [BDNG01] apply, for instance, an adaptive shaping to the selective excitation of molecular mixtures.

The effects of surroundings were first addressed in studies within optimal control schemes incorporating a single bath degree-of-freedom by Bartana et al. [BKT97], and also in local control schemes by Batista and Brumer [BB02]. However, it is worthwile to explore control processes in denser media, where most chemical reactions take place. In particular it is interesting to study the effects of elastic versus inelastic collisions. Different methods for describing influences of a surrounding are available [Wei99]. For example, random fluctuations represented by stochastic noise can be included in the system's Hamiltonian to investigate the effect of incoherent perturbations on photo-ionisation [SR07]. Also, an approach based on the stochastic Schrödinger equation to describe open quantum systems was introduced by Dalibard et al. [DCM92].

The focus of this thesis lies on the application of a Kinetic-Monte-Carlo algorithm to describe the bath influence on control processes [MM99a]. Within this approach, the quantum dynamics for a many-level system coupled to a reservoir is determined via a stochastic Schrödinger equation. As a model system we regard electronic transitions in the sodium dimer molecule, which has been studied extensively both, experimentally and theoretically. Detailed experimental studies on the femtosecond-pulse induced ionisation of Na_2 were performed by Baumert et al. [BGTG91] and modeled by Meier et al. [MW95]. Having theoretically constructed a control field which selectively transfers population from the ground to the first excited electronic state without populating other states, we study the influence of

collisions on the efficiency of the control process, thereby characterising the influence of elastic and inelastic collisions separately.

This thesis is organised as follows: the fundamental theoretical concepts such as electromagnetic field properties, quantum mechanical principles and the basics about system-bath couplings are described in chapter 2. Chapter 3 guides through the numerical methods while, as a first example, a simple relaxation process is treated in chapter 4. Examinations on several aspects of the influence on quantum control systems are presented in chapter 5. The discussion and an outlook are given in chapters 6 and 7.

2. Fundamentals

A brief summary of basic principles is given here, about electromagnetic radiation, the formalism of quantum mechanics guiding to dynamics, the local control theory to derive tailored pulses and open quantum systems incorporating an environment. Hartree units will be used in mathematical derivations throughout this work, see appendix A on page 89.

2.1. Electromagnetic fields

In this section electromagnetic (EM) fields and their effect on matter are discussed. A mathematical formalism to derive plane waves that give a solution to Maxwell's equations, is described and a light pulse represented as a Gaussian wavelet brought to mind. An interaction term $W(t)$ is introduced between an EM field and matter.

2.1.1. Field properties

Electromagnetic interactions give rise to the relevant forces in atomic ranges (see figure 2.1), since molecular dimensions are larger than one Ångström (10^{-10} m), whereabouts weak and strong interaction have already lost their influence. In vacuum electromagnetic radiation obeys *Maxwell's equations*

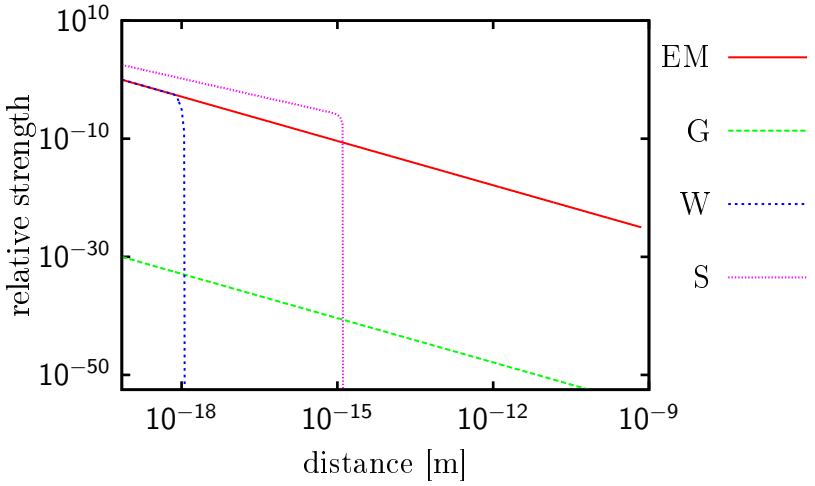

Figure 2.1.: Fundamental forces in the Grand Unified Theory, reproduced from [Pj07] with permission Wiley VCH: Electromagnetic (EM) interactions play an important role in atomic ranges (10^{-10} m), yet gravity (G) is much weaker and molecules are out of reach of intra-nuclear weak (W) or strong (S) interactions.

introduced by James Clerk Maxwell in 1862 [Max62].

$$\begin{aligned}
\vec{\nabla} \cdot \vec{E}(\vec{x}, t) &= 0 \\
\vec{\nabla} \cdot \vec{B}(\vec{x}, t) &= 0 \\
\vec{\nabla} \times \vec{E}(\vec{x}, t) &= -\frac{\partial}{\partial t} \vec{B}(\vec{x}, t) \\
\vec{\nabla} \times \vec{B}(\vec{x}, t) &= \mu_0 \varepsilon_0 \frac{\partial}{\partial t} \vec{E}(\vec{x}, t)
\end{aligned} \tag{2.1.1}$$

Here $\varepsilon_0 = \mu_0^{-1} c^{-2}$ denotes the permittivity of free space, μ_0 the vacuum permeability and c the speed of light, while $\vec{\nabla}$ is the Nabla operator. In the absence of particles and under the adequate gauge, where the scalar potential $\Phi(\vec{x}, t)$ vanishes, a free light field can be derived from a vector

potential $\vec{A}(\vec{x}, t)$ in Cartesian coordinates $\vec{x} = (x, y, z)$.

$$\begin{aligned} -\frac{\partial}{\partial t}\vec{A}(\vec{x}, t) &= \vec{E}(\vec{x}, t) \\ \vec{\nabla} \times \vec{A}(\vec{x}, t) &= \vec{B}(\vec{x}, t) \end{aligned} \tag{2.1.2}$$

The vector potential can be written as a plane wave:

$$\vec{A}_k(\vec{x}, t) = \vec{A}_{k0} \cos(\vec{k}\vec{x} - \omega_k t) \tag{2.1.3}$$

With the direction of propagation along the wave vector $\vec{k}$, whose norm is $|\vec{k}| = \omega_k c^{-1}$, the wave's frequency divided by the speed of light. Each individual wave characterised by the vector $\vec{k}$ follows the wave equation

$$\left(\frac{1}{c^2}\frac{\partial^2}{\partial t^2} - \vec{\nabla}^2\right) \vec{A}(\vec{x}, t). \tag{2.1.4}$$

Inserting a plane wave into the equations (2.1.2) leads to electric $\vec{E}(\vec{x}, t)$ and magnetic field components $\vec{B}(\vec{x}, t)$ mutually perpendicular to each other

$$\begin{aligned} \vec{E}(\vec{x}, t) &= \vec{e}_x \sum_k E_{kx} \sin(\vec{k}\vec{x} - \omega_k t) \\ \vec{B}(\vec{x}, t) &= \vec{e}_y \sum_k B_{ky} \sin(\vec{k}\vec{x} - \omega_k t) \end{aligned} \tag{2.1.5}$$

and the fact that $E_{kx} = -\omega_k |\vec{A}_{k0}|$ and $B_{ky} = -|\vec{k} \times \vec{A}_{k0}|$ are constants with the field mode amplitude $\vec{A}_{k0}$. Assuming a linear polarised E-field along the x-axis propagating in the z-direction, there is no electric component in y-direction $E_{ky} = 0$, for the magnetic component $B_{kx} = 0$ likewise in x-direction [Muk95]. The ratio

$$\frac{E_{kx}}{B_{ky}} = \frac{\omega_k}{|\vec{k}|} \Longrightarrow E_{kx} = c \cdot B_{ky} \gg B_{ky} \tag{2.1.6}$$

reveals that the influence of an electric field is of the amount of $c \approx 137$ in atomic units larger than the magnetic one [BJ03]. Thus, in most cases, the electric component of equation (2.1.5) is sufficient to describe EM field-matter interaction.

The system treated in this thesis is a diatomic molecule in which an optical transition takes place. Since molecules are much smaller than the wavelength of visible light, the position dependence of electromagnetic fields can be neglected [BS03b]. The wavelength is an estimate

$$\lambda = \frac{2\pi}{|\vec{k}|} \approx 380\,\text{nm} - 750\,\text{nm} \gg 303\,\text{pm}. \tag{2.1.7}$$

This is much larger in the visible range than the bond length of a molecule, e.g., the sodium dimer with 303 pm. Therefore this approximation will be applied in the following.

In general a coherent laser pulse can be written as a superposition of several plane waves of the form in equation (2.1.5), to achieve temporal wave trains by interfering constructively or destructively. EM-radiation, in particular a laser pulse, which is a temporally finite electromagnetic wave, is able to interact with molecules under certain circumstances. Special characteristics of a laser are its polarisation, a carrier frequency and coherence [Mai60]. Coherence describes a property of waves in order to receive static interference with other waves, given that they have a fixed phase relation. A Taylor series of a temporal phase, generally around a time t_0, looks like

$$\phi(t) = \sum_{j=0}^{\infty} \frac{a_j}{j!}(t - t_0)^j = a_0 + a_1(t - t_0) + \frac{a_2}{2}(t - t_0)^2 + ... \tag{2.1.8}$$

In this equation a_0 represents an absolute phase and a_1 is of unit frequency. Analogously a frequency dependent phase can be written as

$$\tilde{\phi}(\omega) = b_0 + b_1(\omega - \omega_0) + \frac{b_2}{2}(\omega - \omega_0)^2 + ... \tag{2.1.9}$$

in which b_0 is an absolute phase and b_1 represents a temporal displacement. At time $t_0 = 0$ the partial derivative of the phase $\frac{\partial\phi(t)}{\partial t}\big|_{t_0} = \omega_0$ results in the carrier frequency ω_0. Figure 2.2 depicts a phase shift of a carrier, at which the absolute phase a_0 is shifted by $\frac{\pi}{2}$. If the second derivative of the phase is non-zero, one speaks of a chirped pulse. Below, the linear dependence of

the phases on time or frequency will play a crucial role [SZ08]. There are only real values of an electric field in time domain, but in frequency domain it has complex values. Following a convention that a field was symmetric,

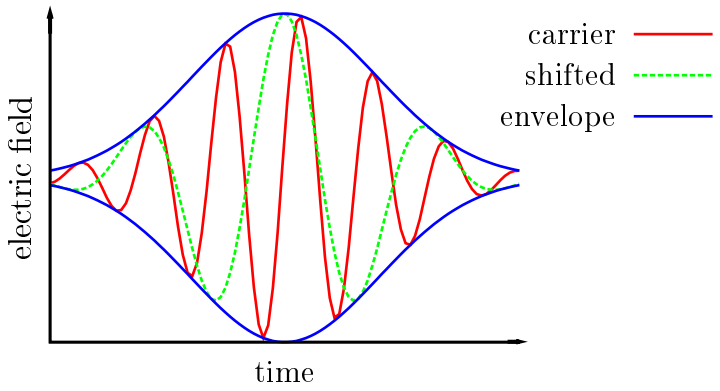

Figure 2.2.: A Gaussian pulse with its envelope (blue) and carrier wave (red). A phase shifted wave (green) is depicted, where $a_0 = \frac{\pi}{2}$.

its complex values equal real-valued negative ones $\vec{\tilde{E}}^{\star}(\omega) = \vec{\tilde{E}}(-\omega)$, hence

$$\vec{\tilde{E}}^{+}(\omega) = \begin{cases} \vec{\tilde{E}}(\omega) & \text{if } \omega \geq 0 \\ 0 & \text{if } \omega < 0 \end{cases}$$

the part of the electric field depending on positive frequencies, fully describes an electric field and is regarded of physical relevance[1]. $\vec{E}(t)$ and $\vec{\tilde{E}}(\omega)$ are connected via a Fourier transform from time into frequency domain as:

$$\begin{aligned} \vec{E}(t) &= \frac{1}{(2\pi)^{1/2}} \int \vec{\tilde{E}}(\omega) e^{-i\omega t} d\omega \\ \vec{\tilde{E}}(\omega) &= \frac{1}{(2\pi)^{1/2}} \int \vec{E}(t) e^{i\omega t} dt \end{aligned} \tag{2.1.10}$$

[1] a $\star$ denotes the complex conjugate (cc)

Describing a laser pulse, the most simple is of Gaussian shape in both domains. Such a modulated superposition of plane waves is called an aperiodic wave train or wavelet. It approaches a spatially and, in an appropriate accuracy, temporally finite experimental laser pulse.

2.1.2. Matter interaction

The electric dipole moment of a distribution of charges q_j at distances $\vec{r}_j$ is:

$$\vec{\mu}(\vec{r}) = \sum_j q_j \, \vec{r}_j \tag{2.1.11}$$

The macroscopic polarisation $\vec{\mathcal{P}}$ can be derived from the sum of these dipole moments per unit volume, so to speak a dipole density [MS07]. The electric dipole interaction energy is:

$$W(\vec{r}, t) = -\vec{\mu}(\vec{r}) \cdot \vec{E}(t) \tag{2.1.12}$$

As stated before, because the wavelength of visible light is much larger than the examined system, the position dependence can be neglected [SO96]. Thus in the electric dipole-approximation the interaction treated here will be an energy of the form of equation (2.1.12) [RZ00].

2.2. Quantum mechanics

In this section the quantum mechanical formalism is introduced [Hei25]. The equation of motion for a quantum mechanical system and a spectral representation of a system's wave function are discussed. Since molecules need to be described quantum mechanically, there are a few quantum mechanical postulates presented in the following.

2.2.1. Formalism

The representation used throughout this thesis shall be the position representation in the Schrödinger picture unless stated differently. Following considerations are performed in one dimension x, extension to several coordinates is straightforward [CTDL91]. A state of a system is entirely quantified by a wave function $\psi(x,t)$. Here, a change of an internal state is restricted to vibronic excitation and relaxation processes. Particle localisation is replaced by a probability density in quantum mechanics of encountering a particle in space. It is defined as $\psi^\star(x,t)\psi(x,t) = |\psi(x,t)|^2$. This interpretation of $\psi(x,t)$ is known as Born's rule [Tan07].

An arbitrary observable $\mathcal{A}$ is a dynamical, measurable and real-valued variable (like position or momentum) and is represented by a linear, self-adjoint operator $\widehat{A}$. The momentum operator $\widehat{p}$ equals $-i\frac{d}{dx}$ and the position operator $\widehat{x}$ is represented by its eigenvalue in this picture. When the domain of self-adjoint operators is equal to their range, those operators are called Hermitian operators.

Operators

Self-adjoint operators can be represented by symmetric matrices $\widehat{A}_{jk} = \widehat{A}^\star_{kj}$

$$\langle\psi_j|\widehat{A}|\psi_k\rangle = \langle j|\widehat{A}|k\rangle = \widehat{A}_{jk} \tag{2.2.1}$$

In Dirac notation $\langle\nu|$ denotes a representation-free bra vector, which is complex conjugate and transposed to the ket vector $|\nu\rangle$. Hermitian operators have real eigenvalues and their eigenfunctions ψ_k are orthonormal to each other, i.e.:

$$\langle\psi_j|\psi_k\rangle \equiv \int \psi_j^\star(x)\psi_k(x)dx = \delta_{jk} \tag{2.2.2}$$

An adjoint operator, symbolised by †, is associated with two operations, a complex conjugation and a transposition $\widehat{A}^\dagger = (\widehat{A}^\star)^T$. If two operators commute, they share a set of common eigenfunctions:

$$\left[\widehat{A},\widehat{B}\right] \equiv \widehat{A}\widehat{B} - \widehat{B}\widehat{A} = 0 \tag{2.2.3}$$

Conserved quantities

One of the most important postulates in physics is conservation of energy in an isolated system. Deduced from an expectation value[2] of an operator

$$\langle \widehat{A} \rangle^n = \frac{\int \psi^* \, \widehat{A} \, \psi dx}{\int \psi^* \psi dx} \tag{2.2.4}$$

a conserved quantity commutes with the time-independent Hamiltonian (see appendix A on page 90). Will say, the expectation value of a not explicitly time dependent quantity is constant in time if its commutator with $\widehat{H}$ vanishes:

$$\frac{d\langle \widehat{A} \rangle}{dt} = \left\langle \frac{\partial \widehat{A}}{\partial t} \right\rangle - i \left\langle \left[\widehat{A}, \widehat{H} \right] \right\rangle = 0 \tag{2.2.5}$$

In practice, measurements of an observable produce a single (sometimes degenerate) eigenvalue of an operator. Operators applied on their eigenfunctions produce eigenvalues and the corresponding equation, for example, for the Hamiltonian reads

$$\widehat{H}|\psi\rangle = \varepsilon|\psi\rangle \tag{2.2.6}$$

which is the time-independent Schrödinger equation. Mathematically, energy eigenvalues ε are diagonal elements of the diagonalised Hamiltonian matrix. A time-dependent Schrödinger equation can be derived consistently from the time-independent one [BR01].

2.2.2. Time-dependent Schrödinger equation

The time-dependent Schrödinger equation reads

$$i \frac{\partial}{\partial t} \psi(x, t) = \widehat{H}(x, \widehat{p}, t) \psi(x, t) \tag{2.2.7}$$

which is mathematically a linear, partial differential equation first order in time of parabolic type [AdP02]. A particle's Hamiltonian (operator) reads

$$\widehat{H}(x, \widehat{p}, t) = \widehat{T}(\widehat{p}) + \widehat{V}(x) + \widehat{W}(x, t) = \widehat{H}_0(x, \widehat{p}) + \widehat{W}(x, t) \tag{2.2.8}$$

[2] normalisation indicated by ^{n}

with $\widehat{W}(x,t)$, which denotes the time-dependent perturbation operator. $\widehat{H}_0(x,\widehat{p})$ is an unperturbed Hamiltonian, which is the sum of kinetic $\widehat{T}(\widehat{p})$ and potential $\widehat{V}(x)$ energy operators. Transitions are induced by photon absorption or emission as the interaction operator in the electric dipole approximation for a z-polarised field is

$$\widehat{W}(x,t) = -\widehat{\vec{\mu}}(x)\cdot\vec{E}(t) = -\widehat{\mu}(x)E(t)\cos\vartheta \tag{2.2.9}$$

Fermi's golden rule

In a system which is disturbed by a temporal infinitely interacting weak field $\vec{E}(t)$, the probability P_{fi} for a transition from an initial $|i\rangle$ to a final state $|f\rangle$ per unit time is given by

$$\lim_{t\to\infty}\frac{d}{dt}\sum_f P_{fi} = 2\pi\sum_f |\langle f|\widehat{\vec{\mu}}|i\rangle|^2\,\delta(\varepsilon_f-\varepsilon_i\pm\omega) \tag{2.2.10}$$

where ε_f and ε_i denote the energies of the final and the initial state, respectively. The rate is proportional to the square of the particular transition dipole matrix element and the δ-function guarantees conservation of energy due to a temporally infinite radiation field. When the photon energy matches the energetic gap between two states, the pulse is called resonant ($\Delta\varepsilon = \varepsilon_f-\varepsilon_i = \pm\omega$). The larger a transition dipole moment, the better is the coupling to an EM field. If $\Delta\varepsilon$ is positive, light will be absorbed, in the negative case stimulated emission is induced.

Time-evolution operator

The quantity $\widehat{U}(t,t_0)$ is called time-evolution operator or sometimes just propagator. It describes a temporal evolution of a system from time t_0 to time t as:

$$|\psi(t_0)\rangle = \widehat{U}(t,t_0)|\psi(t)\rangle \tag{2.2.11}$$

with

$$\widehat{U}(t,t_0) = e^{-i\int_{t_0}^{t}\widehat{H}(t')dt'} \approx e^{-i\widehat{H}(t)(t-t_0)}. \tag{2.2.12}$$

This approximation is valid if $\widehat{H}(t)$ varies negligibly during the time increment $dt = (t - t_0)$. For a time-independent Hamiltonian the time-evolution of a wave function is exact, but for a non commuting Hamiltonian $[\widehat{H}(t), \widehat{H}(t')] \neq 0$ there is a worry about time order. In the latter case propagation is only valid for infinitesimal times, why $\widehat{U}$ is sometimes called *short time propagator*. When the propagator acts on eigenstates of the Hamiltonian, the state is multiplied with a time-dependent phase [PL66].

Basis set expansion

A classical particle is localised, as opposed to a quantum mechanical wave function that is used to describe a system. A coherent superposition of wave functions is called a wave packet which can be localised as well, restricted only by Heisenberg's uncertainty principle. The ability to superpose wave functions in simple sums follows from the homogeneity and linearity of the Schrödinger equation. A wave packet of a pure state can be decomposed into a basis set, also called a spectral representation with coefficients $c_m(t) \in \mathbb{C}$

$$|\psi(t)\rangle = \sum_m c_m(t)|\chi_m\rangle \tag{2.2.13}$$

The squared absolute value of the coefficients $c_m^\star(t)\, c_m(t) = |c_m(t)|^2$ is called population of this state. If interferences between different states exist

$$\langle\psi_1(t)|\psi_0(t)\rangle = \sum_n \sum_m c_{1n}^\star(t) c_{0m}(t) \langle\tilde{\chi}_n|\chi_m\rangle \tag{2.2.14}$$

then coherences denote $c_{1n}^\star(t)\, c_{0m}(t)$. In a density matrix representation, these coherences would be the off-diagonal elements, whereas populations are the diagonal ones, as will be elucidated in section 2.5.2 on page 31.

2.3. Quantum Dynamics

In this section, the dynamics of a quantum mechanical system will be discussed. In describing the evolution of a molecule, one uses the fact that nuclei can be regarded as fix on time scales in which electrons move. Thus, an adiabatic separation in a nuclear and an electronic Schrödinger equation is introduced. The latter relies on coordinates of nuclei parametrically as they appear to be fix [BH54]. Solving the electronic Schrödinger equation leads to adiabatic potentials $V_j(R)$, which enter into the nuclear Schrödinger equation.

2.3.1. Born-Oppenheimer approximation

Even a simple molecule, like a dimer consisting of two equal atoms, can only be described approximately, since one can not solve its time-evolution analytically. The approach often used in theoretical chemistry is the Born-Oppenheimer approximation to describe the dynamics of a system. The Hamiltonian reads

$$\widehat{H}_0 = \widehat{T}_{nuclei} + \widehat{T}_{electrons} + \widehat{V} \tag{2.3.1}$$

$\widehat{V}$ denotes the complete potential energy, while kinetic energies $\widehat{T}$ are composed of nuclear and electronic parts (see appendix A on page 91). Inasmuch electrons are faster than nuclei – for instance, an optical electronic transition takes $\frac{1}{2\Delta\omega} \leqslant \Delta\tau \approx 10^{-15}\,\mathrm{s}$ (compare appendix A on page 92), whereas a vibrational period of the nuclei in a sodium dimer is $\approx 3 \cdot 10^{-13}\,\mathrm{s}$ – one could expect nuclei to be fix ($\widehat{T}_{nuclei} = 0$) during electronic transitions [BO27]. The total wave function of this ansatz summed over electronic and vibrational quantum numbers j, k reads

$$\Psi(r, R, t) = \sum_{j,k} F_{jk}(t)\chi_{jk}(R)\varphi_j(r, R) \tag{2.3.2}$$

with the function $F_{jk}(t)$ containing the time-evolution and the functions $\chi_{jk}(R)$ depending simply on nuclear coordinates R. The *electronic Schrö-*

dinger equation for fixed nuclei reads:

$$(\widehat{T}_{electrons} + \widehat{V})\,\varphi_j(r,R) = V_j(R)\,\varphi_j(r,R) \tag{2.3.3}$$

Eigenvalues $V_j(R)$ in this equation are adiabatic potential hypersurfaces and $\varphi_j(r,R)$ represent orthonormal electronic eigenfunctions. Electronic states $\varphi_0(r,R)$ and $\varphi_1(r,R)$ will be referred to as $|0\rangle$, $|1\rangle$ respectively. The quintessence of the *Born-Oppenheimer approximation* is that non-adiabatic kinetic coupling terms, the off-diagonal elements of the kinetic energy, are set to zero. Nuclear motion is regarded in single electronic states in what follows. There is no coupling to other electronic states and so the nuclear Schrödinger equation reads

$$(\widehat{T}_{nuclei} + V_j(R))\chi_{jk}(R) = \varepsilon_{jk}\chi_{jk}(R) \tag{2.3.4}$$

where $\chi_{jk}(R)$ are nuclear eigenfunctions in electronic states $|j\rangle$ and ε_{jk} are eigenenergies. Nuclear time-dependent wave packets are superpositions as

$$\psi_j(R,t) = \sum_k F_{jk}(t)\chi_{jk}(R) \tag{2.3.5}$$

in which the time-evolution is identified as $F_{jk}(t) = c_{jk}(t)\,e^{-i\varepsilon_{jk}t}$. Within the Born-Oppenheimer approximation, the nuclear dynamics in different electronic states is coupled exclusively by the external field. The internuclear distance R is referred to as reaction coordinate or simply distance in the following. Matrix elements of the dipole operator $\widehat{\mu}$ read

$$\langle\Psi|\widehat{\mu}|\tilde{\Psi}\rangle \approx \langle\chi_{jk}|\chi_{lm}\rangle_R \cdot \langle\varphi_j|\widehat{\mu}_e|\varphi_l\rangle_r \tag{2.3.6}$$

with the electronic part of the dipole operator $\widehat{\mu}_e$, whose dependence on the nuclear distance is neglected furthermore (see appendix A on page 92). The squared norm of the overlap integral $|\langle\chi_{jk}|\chi_{lm}\rangle_R|^2$ between vibrational eigenfunctions of different electronic states is called Franck-Condon (FC) factor. Five overlap factors – the pure integral – of the sodium dimer

overlap	factors
$\chi_{00} - \chi_{10}$	0.0269726
$\chi_{00} - \chi_{11}$	-0.0665701
$\chi_{00} - \chi_{12}$	0.119130
$\chi_{00} - \chi_{13}$	-0.177621
$\chi_{00} - \chi_{14}$	0.234322

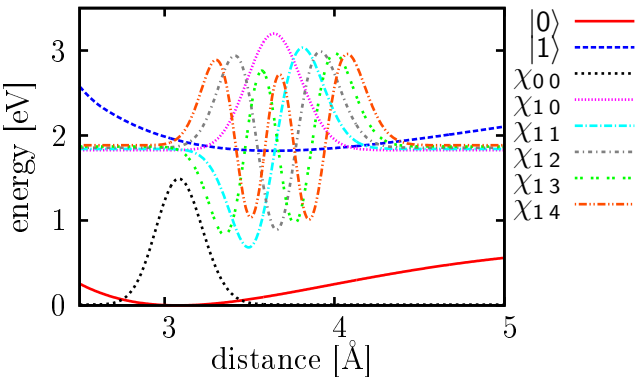

Figure 2.3.: Overlap factors for $|1\rangle \leftarrow |0\rangle$ transitions in the sodium dimer. The electronic ground state potential $|0\rangle$ and the vibrational ground eigenfunction χ_{00} are displayed, as well as the electronic excited state potential $|1\rangle$ and its first five vibrational eigenfunctions. Franck-Condon factors represent the squared absolute of the overlap integral, a measure for the transition probability.

molecule are tabularly shown in figure 2.3, where the first indices are electronic followed by vibrational quantum numbers. In the graph on the right, ground $|0\rangle$ and excited state $|1\rangle$ potential surfaces are shown, with their respective vibrational eigenfunctions. A so called overlap matrix will be used below, consisting of overlap factors for a two level system.

The *Franck-Condon principle* is responsible for vertical transitions from an electronic state to another one. There is no change in coordinates during an interaction, due to immobile nuclei. Transitions can occur between vibrational levels of different electronic states, called vibronic transitions. The symmetry of the states affects whether a projection of a field on $\vec{\mu}$ is parallel ($\cos\vartheta$) or perpendicular ($\sin\vartheta$) [Grä05]. The dipole moment operator of a homo-nuclear molecule has only non-zero values in the off-diagonal parts, coupling elements of electronic states. Written in matrix form in the basis set of electronic eigenfunctions, the off-diagonal elements of the electric dipole (moment), i.e. the *transition dipole moment* $\widehat{\vec{\mu}}_{nm}$, enter into

the field-matter interaction term. For a three state system and parallel transitions, one has

$$\widehat{W}(t) = -\widehat{\vec{\mu}} \cdot \vec{E}(t) = -\begin{pmatrix} 0 & \widehat{\mu}_{01} & \widehat{\mu}_{02} \\ \widehat{\mu}_{10} & 0 & \widehat{\mu}_{12} \\ \widehat{\mu}_{20} & \widehat{\mu}_{21} & 0 \end{pmatrix} \cdot E(t)\cos\vartheta \tag{2.3.7}$$

Here $\widehat{\vec{\mu}}$ is considered as independent of nuclear coordinates (Condon approximation), so that the perturbation $\widehat{W}(t)$ is distance independent as well.

2.4. Local control theory

In this section, a mathematical formalism to derive a tailored electric field will be presented. The coherent control of a chemical reaction shall be of interest here, hence manipulation and control of the outcome is the goal to achieve [ME07]. Two types of interaction of a system with an external electromagnetic field will be discussed in detail.

2.4.1. Derivation

Local control theory was first proposed by Kosloff et al. [KRG+89], for a recent review see [EMT09]. It is a theoretical scheme in which laser pulses induce excitations including the dynamics of a system instantaneously. The goal is to influence an interaction $\widehat{W}(t)$ that a transition from an initial state $|0\rangle$ to a target state $|1\rangle$ takes place. Within a *local* scheme, the control field is constructed such that it takes the instantaneous response of a system into account. Vibronic excitation was the aim of experimental

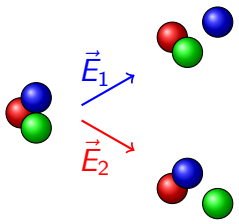

Figure 2.4.: Scheme of a selective reaction by different fields.

methods [BS92] as well as theoretical algorithms [Ban94]. The mathematical ansatz is to take an arbitrary, time-independent operator $\widehat{A}$ and evaluate its rate using equation (2.2.7), the time-dependent Schrödinger equation, the following way:

$$\begin{aligned}
\frac{d\langle\widehat{A}\rangle}{dt} &= \frac{d}{dt}\langle\Psi(t)|\widehat{A}|\Psi(t)\rangle \\
&= \langle\frac{\partial}{\partial t}\Psi(t)|\widehat{A}|\Psi(t)\rangle + \langle\Psi(t)|\widehat{A}|\frac{\partial}{\partial t}\Psi(t)\rangle \\
&= i\langle\Psi(t)|\widehat{H}(t)\widehat{A}|\Psi(t)\rangle - i\langle\Psi(t)|\widehat{A}\widehat{H}(t)|\Psi(t)\rangle \\
&= i\langle\Psi(t)|\left[\widehat{H}(t),\widehat{A}\right]|\Psi(t)\rangle
\end{aligned}$$

Here, the commutator between the Hamiltonian and $\widehat{A}$ appears. Furthermore Malinovsky et al. recommend [MMT97] to split the system in an unperturbed and perturbed part:

$$\frac{d\langle\widehat{A}\rangle}{dt} = i\langle\Psi(t)|[\widehat{H}_0,\widehat{A}]|\Psi(t)\rangle + i\langle\Psi(t)|[\widehat{W},\widehat{A}]|\Psi(t)\rangle \tag{2.4.1}$$

If the arbitrary operator is a conserved quantity, that is, it commutes with $\widehat{H}_0$, the rate reduces to

$$\Rightarrow \quad \frac{d\langle\widehat{A}\rangle}{dt} = -\vec{E}(t)\, i\,\langle\Psi(t)|[\widehat{\vec{\mu}},\widehat{A}]|\Psi(t)\rangle$$

Consequently, the rate can be controlled by the choice of the EM field. In this equation the perturbation operator is considered as described earlier (see eq. (2.2.9)).

Population transfer

If $\widehat{A}(t)$ is a projector $|k\rangle\langle k|$, the population and depopulation of a state $|k\rangle$ is characterised by the rate

$$\begin{aligned}
\frac{d\langle\widehat{A}(t)\rangle}{dt} &= \frac{d}{dt}\langle\Psi(t)|k\rangle\langle k|\Psi(t)\rangle \\
&= -\vec{E}(t)\, i \sum_m \langle\psi_m(t)\,|[\widehat{\vec{\mu}}, |k\rangle\langle k|]|\Psi(t)\rangle \\
&= -\vec{E}(t)\, i \sum_m \langle\psi_m(t)|\widehat{\vec{\mu}}_{mk}|\psi_k(t)\rangle - \langle\psi_k(t)|\widehat{\vec{\mu}}_{km}|\psi_m(t)\rangle \\
&= -2\cdot\vec{E}(t)\sum_m \Im\left\{\langle\psi_k(t)|\widehat{\vec{\mu}}_{km}(t)|\psi_m(t)\rangle\right\}
\end{aligned}$$

where $\Im$ denotes the imaginary part. If a field of the size

$$\vec{E}(t) := -E_0 \sum_m \Im\left\{\langle\psi_k(t)|\widehat{\vec{\mu}}_{km}|\psi_m(t)\rangle\right\} \tag{2.4.2}$$

is chosen, the rate is always positive and an excitation into target state $|k\rangle$ will be executed monotonically. The size of the control field amplitude E_0 can accelerate the process to a certain extent. Clearly, an initial population (seed) in $|k\rangle$ is required in a numerical simulation, otherwise the field remains zero at all times and no transition takes place.

Rabi oscillations

Strong laser fields are able to periodically transfer population between two different states (see Fig. 2.5 on the next page). The periodic exchange of energy between a resonant external field and a two-level system can be interpreted as photon absorption and stimulated emission. The system's population oscillates between the two states with half a Rabi-frequency $\Omega_R = E_0\langle f|\widehat{\mu}|i\rangle$. Laser pulses are often characterised by the pulse area $A = \Omega_R\, t$. A complete population transfer can be described by an $(A =)\frac{\pi}{2}$-pulse with half a Rabi-oscillation [AF05]. The local control scheme presented here does not rely on non-linear dynamics and enormous intensities E_0.

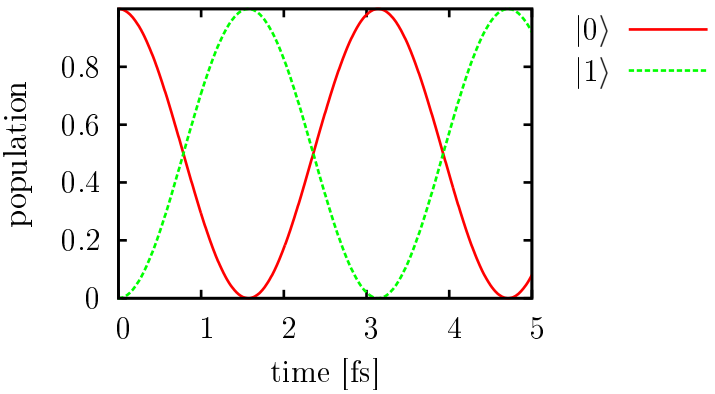

Figure 2.5.: Population oscillates between state $|i\rangle$ and $|f\rangle$ under the influence of strong electromagnetic fields (Rabi oscillations).

In contrast, a control field as in equation (2.4.2) is adapted to system dynamics.

Dissipation

Dissipation describes the process in which a physical system swaps energy with a surrounding environment in form of thermal energy, for example. A similar approach as for a population transfer can be used to pump energy into the system (heat) or out of the system (cool) by an electromagnetic field. When energy is examined in LCT, the operator $\widehat{A}$ is given by the unperturbed Hamiltonian $\widehat{H}_0$

$$\begin{aligned}\frac{d\langle\widehat{H}_0\rangle}{dt} &= i\langle\Psi(t)|[\widehat{H}(t),\widehat{H}_0]|\Psi(t)\rangle \\ &= -i\,E(t)\langle\Psi(t)|[\widehat{\mu},(\widehat{T}+\widehat{V}(R))]|\Psi(t)\rangle.\end{aligned}$$

In case of a linear dipole moment $\widehat{\mu} \propto R$, it commutes with $\widehat{V}(R)$, and the kinetic part simplifies to

$$\begin{aligned} &= i\,E(t)\frac{q}{2m}\left\langle \Psi(t)\left|\left[R,\frac{d^2}{dR^2}\right]\right|\Psi(t)\right\rangle \\ &= -i\,E(t)\frac{q}{m}\left\langle \Psi(t)\left|\frac{d}{dR}\right|\Psi(t)\right\rangle \\ &= E(t)\frac{q}{m}\langle\widehat{p}\rangle(t) \end{aligned} \tag{2.4.3}$$

where m is the reduced mass of the system. The rate of the energy expectation value will be influenced if one defines $E(t) := \lambda\langle\widehat{p}\rangle$ and picks the λ as ± 1. This means, the system will heat up or relax in the case $\lambda = +1$ or $\lambda = -1$, respectively (see appendix A on page 91).

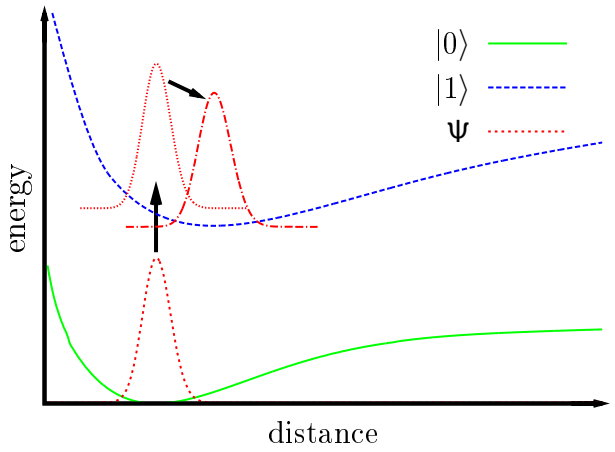

Figure 2.6.: Vertical excitation from ground $|0\rangle$ to excited state $|1\rangle$ followed by a relaxation (cooling) of the excited wave packet during its oscillatory propagation.

Matter in thermal equilibrium

A system in thermal equilibrium can be assigned a temperature, in other words an energy value. The loss or gain of energy is performed by absorption or emission processes. The rates k_{nm} of absorption and emission k_{mn}

between two states $|n\rangle$ and $|m\rangle$ of such a system resemble if the condition

$$k_{nm}\, e^{\frac{\varepsilon_m}{k_B T}} = k_{mn}\, e^{\frac{\varepsilon_n}{k_B T}} \tag{2.4.4}$$

is fulfilled, with the Boltzmann constant k_B. A canonical ensemble, in which a system coupled to a reservoir with temperature T, is being in a state $|n\rangle$ with energy ε_n and a probability

$$P_n = \frac{1}{Z} e^{-\varepsilon_n / k_B T} \tag{2.4.5}$$

with the partition function $Z = \sum_n e^{-\varepsilon_n / k_B T}$. That is, these rates k_{nm}, k_{mn} are responsible for an energetic (population) exchange between different levels.

2.5. Open quantum systems

This section is devoted to the quantum mechanical treatment of a system in its environment. Introducing the concept of fluctuations via a quantum Langevin approach, a system-bath-model is used to describe dissipative processes. A density operator representation guides via the Liouville-von-Neumann equation in the interaction picture to the master equation in the Schrödinger picture. The comparison of a density matrix and a Monte-Carlo wave function justifies the use of the phenomenological stochastic Schrödinger equation in the end.

2.5.1. Langevin equation

The Hamiltonian function of a classical, free particle, which is to be decelerated by an external electric field $E(t)$, reads in one dimension

$$\mathsf{H} = \frac{p^2}{2m} - x\, E(t). \tag{2.5.1}$$

The field is non-conservative, because $E(t) = \xi v$ is proportional to the particle velocity $v = \frac{dx}{dt}$ (compare equation (2.4.3)) with a damping co-

efficient ξ. This classical friction means a loss of norm in quantum mechanics [Kam01]. So another term is missing, introducing the heuristic Langevin equation [Kam97], which originally described Wiener processes like Brownian motion:

$$m\frac{d^2x}{dt^2} = -\xi v + L(t). \tag{2.5.2}$$

A fluctuating term $L(t)$ fulfils the so called Markovian condition, this is, the system does not memorise any situations before [Car93]:

$$\langle L(t)L(t')\rangle = 2C\delta(t-t') \tag{2.5.3}$$

Postulates

- Damping shall be linear in $-v$, so the fluctuation shall be in opposite direction to the movement of a particle.
- There is a fluctuating term with the property $\langle L(t)\rangle = 0$ (1. moment), thus taking averages the fluctuation shall not contribute
- and being Markovian, i.e. infinite correlation time between fluctuations, therefore fluctuations at two different time steps shall not be related.

From the equipartition theorem of statistical mechanics and thermodynamics is known that $\frac{m}{2}\langle v^2\rangle = \frac{1}{2}k_B T$. I.e., for particles in one dimension (ideal gas), the mean squared velocity of particles is proportional an ensemble's temperature and so called white noise has a property

$$\langle L(t)L(t')\rangle = 2\xi k_b T\delta(t-t'). \tag{2.5.4}$$

The magnitude of fluctuations becomes $C = \xi k_B T$, which is the so called Fluctuation-Dissipation-Theorem in thermodynamical equilibrium [Ris84], for which

$$\langle v^2\rangle = \lim_{t\to\infty}\left\langle\left(\frac{dx}{dt}\right)^2\right\rangle \tag{2.5.5}$$

is valid. The Fluctuation-Dissipation-Theorem states that external perturbations to a system can be expressed by its fluctuation properties in linear response theory [Wei99].

Quantum dynamical relation

An imaginary damping term in the Schrödinger equation leads to a real-valued propagator and consequently violates the conservation of probability. The Hamiltonian for the former introduced formalism reads

$$\widehat{H} = \widehat{H}_0 - \underbrace{i\widehat{Q}}_{damping} + \underbrace{i\widehat{L}(t)\widehat{F}}_{noise} \tag{2.5.6}$$

with the requirement $2\widehat{Q} = \widehat{F}^\dagger\widehat{F}$ [HJC95]. If $\widehat{Q}$ is Hermitian, the short time-evolution would look like $\widehat{U}(dt) \approx e^{i(\widehat{H}_0 - i\widehat{Q})dt}$ (compare section 2.2.2), coming from[3]

$$\begin{aligned}\langle\Psi(t+dt)|\Psi(t+dt)\rangle &= \langle\Psi(t)|\Psi(t)\rangle_x - 2dt\langle\Psi(t)|\widehat{Q}|\Psi(t)\rangle_x \\ &+ dt\langle\Psi(t)|\widehat{F}^\dagger\widehat{F}|\Psi(t)\rangle_x + \mathcal{O}(dt^2).\end{aligned} \tag{2.5.7}$$

So the norm of $\Psi(t)$ is conserved in the order dt leading to a stochastic quantum Langevin equation:

$$-i\frac{\partial}{\partial t}\Psi = \widehat{H}_0\Psi - i\sum_\alpha \widehat{Q}_\alpha\Psi + iL_\alpha(t)\widehat{F}_\alpha\Psi \tag{2.5.8}$$

In this equation α represents different realisations inspected closely in the next subsection.

2.5.2. Stochastic wave functions

A stochastic process in physical parlance is a random function of which one variable is time [GZ00]. An ensemble is the realisation of those processes

[3] $_x$ means at a constant arbitrary coordinate x

that means an expectation value is represented by the law of large numbers

$$\langle \widehat{A} \rangle = \lim_{N\to\infty} \overline{A}_N = \lim_{N\to\infty} \frac{1}{N} \sum_{n=1}^{N} A_n \tag{2.5.9}$$

$\overline{A}_N$ is the ensemble average and A_n the occurence or trajectory of path n. A quantum mechanical mean value is determined via

$$\langle \widehat{A} \rangle \equiv \sum_{\alpha} P_\alpha \langle \psi_\alpha | \widehat{A} | \psi_\alpha \rangle \tag{2.5.10}$$

so P_α represents the probability of a realisation α. The sum over all realisation probabilities shall be unity $\sum_\alpha P_\alpha = 1$. If a run's $|\psi_\alpha\rangle$ is a system's pure state, the projector equals its square $|\psi_\alpha\rangle\langle\psi_\alpha|\psi_\alpha\rangle\langle\psi_\alpha| = |\psi_\alpha\rangle\langle\psi_\alpha|$. Additionally, since $|\psi_\alpha\rangle\langle\psi_\alpha|$ is Hermitian, one can expand

$$|\psi_\alpha\rangle\langle\psi_\alpha| = \sum_{j,j'} c_{j'}^{\alpha\star}(t) c_j^\alpha(t) |j'\rangle\langle j| \tag{2.5.11}$$

into the spectral representation given by a basis in eigenvectors $|j\rangle$ with their time-dependent coefficients $c_j^\alpha(t)$. The density operator is given by

$$\frac{1}{N} \sum_{\alpha=1}^{N} |\psi_\alpha\rangle\langle\psi_\alpha| \equiv \sigma \tag{2.5.12}$$

if the ensemble is large enough while summing up different realisations. Dalibard et al. [DCM92] emphasised quantum trajectories as a tool to simulate the time-evolution of dissipative quantum optical systems. The key is to sum up different realisations and draw the mean out of a representative statistical ensemble, in which accuracy is achieved by the number of the simulated runs. In general, stochastic processes - unlike deterministic ones - do not lead to the same results. But if conducted several times, they should approximate a non-deterministic treatment satisfactorily [Gar09].

2.5.3. System-reservoir-approach

A standard scheme to describe dissipation or irreversible behaviour when a system, traditionally denoted S, and a reservoir B interact is a system-bath approach. Moreover, S is typically spatially confined, B is infinitely

extended and so more indefinable. By effect of the interaction, energy will irretrievably flow from system S to bath B. A canonical ensemble represents a system with a constant volume and fixed number of particles in thermal equilibrium with a reservoir. Gradual evolution into an equilibrium state is called a relaxation process and such relaxation phenomena are irreversible processes [Blu96]. Initially S and B are assumed to be uncoupled and factorise

$$|\Psi(t=0)\rangle = |\psi_S(r,0)\cdot\psi_B(R,0)\rangle \tag{2.5.13}$$

A coupling causes the composite state to be an entanglement of both wave functions. The time-evolution of the system is of interest influenced by quantum noise. A useful description requires reproduction of results by statistical mechanics and consistency in energy and norm. The Hamiltonian including system $\widehat{H}_S(r)$, bath $\widehat{H}_B(R)$ and their interaction $\widehat{J}(r,R)$ reads

$$\widehat{H} = \widehat{H}_S(r) + \widehat{H}_B(R) + \widehat{J}(r,R) \tag{2.5.14}$$

The trace Tr_R over the reservoir of the system-reservoir density operator $\sigma(r,R,t)$ leads to a reduced density operator $\rho(r,t)$ containing all the information needed to analyse the problem:

$$\rho(r,t) \equiv Tr_R\{\sigma(r,R,t)\} = \sum_n \langle\psi_n(R)|\sigma(r,R,t)|\psi_n(R)\rangle_R \tag{2.5.15}$$

The goal to achieve is describing the system's evolution, without further notice of the bath's. Thus a changeover into the interaction picture is helpful. The Schrödinger picture's interaction $\widehat{J}(r,R)$ reads in the interaction picture, marked $^{\Im}$:

$$\widehat{J}^{\Im}(r,R,t) = e^{i\widehat{H}_0 t}\widehat{J}(r,R)e^{-i\widehat{H}_0 t} \tag{2.5.16}$$

At which the equation of motion (Liouville-von Neumann) reads accurate to second order

$$\frac{\partial}{\partial t}\rho^{\Im}(r,t) = -iTr_R\{[\widehat{J}^{\Im}(r,R,t),\sigma(r,R,0)]\} + \frac{1}{i^2}\int_0^{t'} Tr_R\{\widehat{J}^{\Im}(r,R,t'),[\widehat{J}^{\Im}(r,R,t),\sigma^{\Im}(r,R,t')]]\}dt'. \tag{2.5.17}$$

The integral denotes the non-Markovian background, where the time t' needs to be long compared to the reservoir memory time. Born's approximation for weak coupling is that the process is irreversible and the system has no influence on the reservoir $\sigma^{\Im}(r,R,t) = \rho^{\Im}(r,t)\,\rho(R,0)$, yet $\rho(R,0)$ is the invariant reduced density operator of the bath. Additionally, the Markov condition is demanded, this means there is an infinite correlation time $\sigma^{\Im}(r,R,t) \neq \sigma^{\Im}(r,R,t')$ between two representations [Loi73]. Taking this into account, the equation of motion can be written as

$$\frac{\partial}{\partial t}\rho^{\Im}(r,t) = -iTr_R[\widehat{J}^{\Im}(r,R,t),\rho(r,0)\,\rho(R,0)] - \int_0^{t} Tr_R[\widehat{J}^{\Im}(r,R,t'),[\widehat{J}^{\Im}(r,R,t),\rho^{\Im}(r,t')\,\rho(R,0)]]dt', \tag{2.5.18}$$

introducing the time-dependent correlation functions $\widehat{\aleph}^{\Im}(r,t)$ and $\widehat{\mho}^{\Im}(R,t)$

$$\begin{aligned}\widehat{J}^{\Im}(r,R,t) &= e^{i(\widehat{H}_S+\widehat{H}_B)t}\sum_n \widehat{\aleph}_n(r)\,\widehat{\mho}_n(R)e^{-i(\widehat{H}_S+\widehat{H}_B)t} \\ &= \sum_n \widehat{\aleph}_n^{\Im}(r,t)\,\widehat{\mho}_n^{\Im}(R,t)\end{aligned} \tag{2.5.19}$$

Since $Tr\{\widehat{\aleph}\widehat{\mho}\} = Tr\{\widehat{\mho}\widehat{\aleph}\}$, the density's derivative can be further simplified, considering the expectation value of the reservoir correlation function

$$\begin{aligned}\langle\widehat{\mho}_n^{\Im}(R,t)\rangle &= Tr_R\{\widehat{\mho}_n^{\Im}(R,t)\rho(R,0)\} \\ &= \sum_m \langle m|\widehat{\mho}_n^{\Im}(R,t)|m\rangle\langle m|\rho(R,0)|m\rangle.\end{aligned}$$

Here, m represent eigenstates of $\widehat{H}_B$ and the invariant reservoir density $\rho(R,0) = \frac{1}{Z}e^{-\widehat{H}_B/k_BT}$ is assumed diagonal (compare eq. (2.4.4)). If $\widehat{\mho}_n^{\Im}$

had diagonal elements – those could already have been included in the free Hamiltonian – then $\langle \widehat{\mho}_n^{\Im}(R,t)\rangle = 0$. Accordingly, time-correlation functions to a bath are

$$\langle \widehat{\mho}_n^{\Im}(R,t)|\widehat{\mho}_j^{\Im}(R,t')\rangle = Tr_R\{\widehat{\mho}_n^{\Im}(R,t)\widehat{\mho}_j^{\Im}(R,t')\rho(R,0)\} \tag{2.5.20}$$

maximal, if the correlation time is $t = t'$, which is forbidden in a Markovian reservoir. Reservoir correlation functions are stationary, because they rely only on the time difference $\langle \widehat{\mho}_n^{\Im}(R,t)\widehat{\mho}_j^{\Im}(R,t')\rangle = \langle \widehat{\mho}_n^{\Im}(R,t-t')\widehat{\mho}_j^{\Im}(R)\rangle$ and hence equation (2.5.18) simplifies to

$$\begin{aligned}\frac{\partial}{\partial t}\rho^{\Im}(r,t) = -\sum_{nj}\int_0^\infty dt''([\widehat{\aleph}_n^{\Im}(r,t),\widehat{\aleph}_j^{\Im}(r,t-t'')\rho^{\Im}(r,t)]\langle \widehat{\mho}_n^{\Im}(R,t'')\widehat{\mho}_j^{\Im}(R)\rangle \\ -[\widehat{\aleph}_n^{\Im}(r,t),\rho^{\Im}(r,t)\widehat{\aleph}_j^{\Im}(r,t-t'')]\langle \widehat{\mho}_j^{\Im}(R)\widehat{\mho}_n^{\Im}(R,t'')\rangle\end{aligned} \tag{2.5.21}$$

All the information about the reservoir is contained in the correlation functions. Inspecting their time evolution and introducing the rates

$$\lambda^+_{mk\ell o} = \sum_{nj}\langle m|\widehat{\aleph}_n^{\Im}|k\rangle\langle \ell|\widehat{\aleph}_j^{\Im}|o\rangle\int_0^\infty dt'' e^{-i(\varepsilon_\ell-\varepsilon_o)t''}\langle \widehat{\mho}_n^{\Im}(t'')\widehat{\mho}_j^{\Im}\rangle \tag{2.5.22}$$

and

$$\lambda^-_{mk\ell o} = \sum_{nj}\langle m|\widehat{\aleph}_j^{\Im}|k\rangle\langle \ell|\widehat{\aleph}_n^{\Im}|o\rangle\int_0^\infty dt'' e^{-i(\varepsilon_m-\varepsilon_k)t''}\langle \widehat{\mho}_j^{\Im}\widehat{\mho}_n^{\Im}(t'')\rangle \tag{2.5.23}$$

then equation (2.5.21) reduces to a Redfield equation (2.5.25) [Red57]. Back in the Schrödinger picture, the net transition rates k_{mo} averaged over the reservoir states are introduced:

$$k_{mo} := \lambda^+_{ommo} + \lambda^-_{ommo} \qquad k_{om} := \lambda^+_{moom} + \lambda^-_{moom}. \tag{2.5.24}$$

These rates represent probabilities per unit time of a transition between $|o\rangle$ and $|m\rangle$ induced by the reservoir. Diagonal elements of the system density matrix are equivalent to those in the interaction picture and states evolve

coherently with the Hamiltonian of the system disturbed by the reservoir

$$\begin{aligned}\langle o|\frac{\partial}{\partial t}\rho(r,t)|m\rangle &= -i\langle o|[\widehat{H}_S,\rho(r,t)]|m\rangle + \delta_{om}\sum_n\langle n|\rho(r,t)|n\rangle k_{mn} \\ &- (\sum_n(\lambda^+_{onno}+\lambda^-_{mnnm}) - \lambda^+_{mmoo} - \lambda^-_{mmoo})\langle o|\rho(r,t)|m\rangle\end{aligned} \tag{2.5.25}$$

The second and third term on the right hand side build up the relaxation superoperator $\Lambda(\rho(r,t))$, describing dissipative effects of the reservoir on the system and must be of so called Lindblad form in order to preserve the trace of a density operator [Lin76] [Wol97]. A comparison with optical Bloch equations reveals that the latter term $\sum_n(\lambda^+_{onno}+\lambda^-_{mnnm}) - \lambda^+_{mmoo} - \lambda^-_{mmoo}$ can be identified as a dephasing rate γ_{om}. The effective irregularity rate is composed of

$$\frac{1}{\tau^*} = \frac{(\Gamma_o+\Gamma_m)}{2} + \gamma_{om} \tag{2.5.26}$$

within which $\Gamma_o = \sum_{n\neq o} k_{on}$ is the total escape rate from state $|o\rangle$ describing the thermal decay and τ^* the mean collision time [Blo46] [AE75]. If the system and the reservoir are in thermal equilibrium (compare eq. (2.4.4)) one can evolve a generalised master equation

$$\frac{d}{dt}\rho_{mm}(r,t) = \sum_{n\neq m} k_{mn}\rho_{nn}(r,t) - \sum_{n\neq m} k_{nm}\rho_{mm}(r,t). \tag{2.5.27}$$

This rate equation is often called Pauli master equation, for the diagonal elements of the system density matrix. It is a central equation in statistical physics for a description of coherent transport into (k_{mn}) or out of (k_{nm}) a system state $|m\rangle$ [ALV02].

Comparison

A density matrix formalism is often used to describe dissipative system-reservoir interactions. Mølmer et al. [MCD93] introduced a Monte-Carlo approach using a stochastic wave function to study time-evolution with

fluctuations by quantum jumps. A quantum-jump approach was examined by Zoller et al. [ZMW87] as a discontinuous change in quantum state. A stochastic treatment of a system evolution can lead to the same results as a direct method. Saalfrank [Saa96] shows that a stochastic approach requires less realisations N than gridpoints M to converge to reliable results and a single realisation scales with $M \log_2 M$. A Liouville-von Neumann approach with a density matrix needs $M^2 \log_2 M$, which leads to a conclusion that this direct approach is less efficient.

A mixed state can not be represented by a linear combination of pure states, thus not by wave functions, i.e. as long as a system is initially in a pure state and imposed to a coherent external field, the system will be in a pure state after laser excitation as well. So a treatment with exclusively wave functions is justified. Breuer et al. [BHP99] go even further: "It will be shown that for sufficiently large N and for any prescribed fixed statistical error the stochastic wave function method is always faster than the integration of the corresponding density matrix equation".

Thus, solving open quantum systems numerically by a stochastic Monte-Carlo approach is more efficient in terms of memory saving. Having said that, a closer view to numerical methods will be appropriate, described in the next chapter.

3. Numerical methods

This chapter is about the numerical approaches to describe dynamics of the system of interest (see figure 3.1). On a computing machine, all calculations are projected into a discrete Hilbert space. A numerical transformation into Fourier space will be introduced as well as the split-operator method. An imaginary time-evolution to derive eigenfunctions of a Hamiltonian is presented. The time-evolution of coefficients on the contrary is done by a Runge-Kutta procedure. Finally the focus lies on the Kinetic Monte-Carlo algorithm and its implementation.

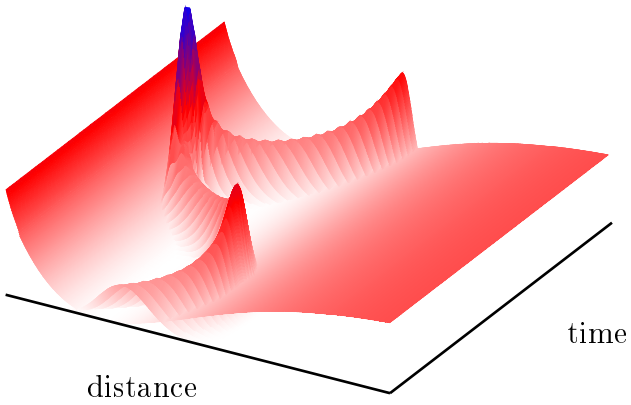

Figure 3.1.: Scheme of a wave function's oscillatory time-evolution in an adiabatic potential curve. The wave packet is focussed on the potential wall's steep side and broadens traversing the potential minimum.

Calculations on a grid

The basic idea of a Fourier-grid method is to represent a wave function on a discrete, equidistant spatial grid for the time-evolution [Kos88]. Wave packets have to be sampled on a number of grid points M, and the finer the mesh, the better is the approach. In this thesis a grid size of $M = 1024$ grid points is chosen, to reach convergent results. The wave packets are subject to periodic boundary conditions, so a discretised wave function is represented as

$$\psi(x) \approx \sum_{k=1}^{M} a_k e^{i2\pi k\Delta x/L} \tag{3.0.1}$$

where $L = x_{end} - x_0 = (M-1)\Delta x$ is the total grid length and a_k is interpreted as momentum space amplitude. Due to the Whittaker-Kotel'nikov-Shannon sampling theorem a maximal momentum $p_{max} < \frac{2\pi}{\Delta x}$ can not be resolved any more via a Fourier transform, so the highest momentum represented is $p_{max} - \Delta p$. Thus an evenly spaced momentum grid is automatically constructed with the momentum increment $\Delta p = \frac{2\pi}{M\Delta x}$ [KK83] (see also appendix A on page 93).

Fast-Fourier transformation

A general Fourier transformation of a wave function is written as

$$\tilde{\psi}(p) = \frac{1}{\sqrt{2\pi}} \int \psi(x) e^{-ipx} dx = \mathcal{FT}[\psi(x)] \tag{3.0.2}$$

$$\psi(x) = \frac{1}{\sqrt{2\pi}} \int \tilde{\psi}(p) e^{ipx} dp = \mathcal{FT}^{-1}[\tilde{\psi}(p)] \tag{3.0.3}$$

Spatially discrete functions on a finite grid with M sampling points require periodicity $\psi(x) = \psi(x + L)$. Thereby no rapid variation of the function in $2L/M$ is permitted in order to resolve all variations. This means, if the sampled function varies less, that is, as long as the variations in Δx are small, it can be reconstructed by the chosen grid. On the other hand, if the periodic function oscillates with a higher momentum than can be resolved

on the grid, the algorithm sets this momentum in the negative regime due to boundary conditions. A discrete Fourier transform was already proposed by Gauß in 1805 *Teoria interpolationis methodo nova tractata* [Rei02]. If the number of sampling points M in a discrete Fourier transform is even, one can half, if $\frac{M}{2}$ is even, yet quarter the effort of calculating. Additionally, for numerical calculations $M = 2^m$ is advantageous. Then a fast Fourier transformation scales with the order $\mathcal{O}(M \log_2 M)$ instead of a pure discrete Fourier transform of the order $\mathcal{O}(M^2)$ in number of operations. A widely used software library called FFTW is implemented to perform the fast Fourier Transformations [FJ05].

3.1. (Symmetric) split-operator method

The short time propagation introduced in section 2.2.2 on page 19 is applied splitting a system's Hamiltonian into a kinetic and a potential part. Since the kinetic energy $\widehat{T}(p)$ contains the momentum operator, one can handle this operator in Fourier space best. The representation change is carried out by a fast Fourier transformation. The potential energy is diagonal in position space, hence the split-operator (SO) technique

$$e^{-i\widehat{H}_0 dt} = e^{-\frac{i\widehat{V}}{2}dt} e^{-i\widehat{T}dt} e^{-\frac{i\widehat{V}}{2}dt} + \mathcal{O}(dt^3) \tag{3.1.1}$$

propagates these parts separately [FFjS82]. Because kinetic and potential energy do generally not commute due to $[\widehat{x}, \widehat{p}] = i$, this is valid to second order in time. The third-order error can be minimised by a short time step dt. To incorporate a transition dipole interaction of the form of equation (2.2.9) a third exponential containing the interaction matrix

$$\widehat{W}(t) = \begin{pmatrix} 0 & \widehat{W}_{01}(t) \\ \widehat{W}_{10}(t) & 0 \end{pmatrix} = \begin{pmatrix} 0 & -\widehat{\mu}_{01}E(t) \\ -\widehat{\mu}_{10}E(t) & 0 \end{pmatrix} \tag{3.1.2}$$

appears. The power series then yields

$$e^{-i\widehat{W}(t)dt} \begin{pmatrix} \cos(\widehat{\mu}E(t))dt & -i\sin(\widehat{\mu}E(t))dt \\ -i\sin(\widehat{\mu}E(t))dt & \cos(\widehat{\mu}E(t))dt \end{pmatrix} \tag{3.1.3}$$

The exponential term is split and applied on the wave function before and after the rest of the propagation. The SO-technique is fast, as long as there are few repetitions, because every time step involves two Fourier transformations. It is a robust and unitary operation (norm conserving), as long as the time-evolution is split into sufficiently small steps $dt = \frac{t-t_0}{N_{steps}}$. Then the time-evolution operator requires no time ordering, but one has to keep in mind the alteration of the perturbation $\widehat{W}$ in dt as well as the energy relation to a time step, see appendix A on page 92, whereupon the maximal resolved energy is $\varepsilon_{max} = \frac{2\pi}{dt}$.

Relaxation method

The symmetric split-operator algorithm can be utilised to calculate eigenstates of a given Hamiltonian. An imaginary time-evolution of an arbitrary initial function is then called relaxation method [KTE86]. A spectral rep-

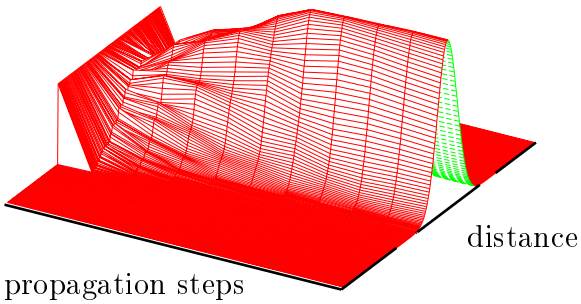

Figure 3.2.: An initial rectangular function serves as a starting point for the relaxation method. Upon imaginary time-evolution the initial function evolves into the ground state wave function.

resentation of a wave function reads

$$\psi = \sum_{n}^{\infty} c_n \chi_n \tag{3.1.4}$$

with the coefficients $c_n = \langle \chi_n | \psi \rangle$ and eigenfunctions χ_n corresponding to eigenvalues ε_n. In the simplest case of relaxation the starting function is

a rectangle as illustrated in figure 3.2. The propagation, damping each eigenstate with a rate depending on its eigenenergy, is written as

$$\psi(\tau + d\tau) = \sum_n \langle \chi_n | \psi(\tau) \rangle e^{-d\tau \varepsilon_n} \chi_n \tag{3.1.5}$$

and is non-unitary, thus the wave function is normalised after each time step $d\tau = i\,dt$. In the limit $\tau \to \infty$ the wave function ψ converges to the ground state χ_0. Next eigenfunctions to eigenenergy ε_m are obtained by projection as:

$$\chi_m = \lim_{\tau \to \infty} \psi(\tau + d\tau) - \sum_{n=0}^{m-1} \langle \chi_n | \psi(\tau) \rangle \, \chi_n \tag{3.1.6}$$

As long as it is included in the initial function, the relaxation method results in the eigenfunction.

3.2. Fourth order Runge-Kutta method

The Runge-Kutta method fourth order (RK4) is an analytical approximation method. Since Taylor expansions require derivatives explicitly, they can not be applied in some cases. The Runge-Kutta method is a four step approximative scheme solving an initial value problem of ordinary differential equations with a given value and slope in the sampling point x_n:

$$y(x_n) = y_n \quad \text{and} \quad y`(x_n) = f(x_n, y_n)$$

The ansatz expanding a function value in the next sampling point $n + 1$ reads

$$y_{n+1} \approx y_n + h \sum_{i=1}^{s} w_i k_i$$

with stepsize h on the abscissa and weights w_i, in doing so

$$k_i := f(x_n + h\alpha_i, y_n + h \sum_{j=1}^{i-1} \beta_{ji} k_j)$$

are recursively defined slopes in $\mathcal{S}$ intermediate steps. All Runge-Kutta methods have $\alpha_1 = 0$ in common and the weights – as well as the coefficients – can be arranged symmetrically to the values in table 3.1 with Simpson's one-third-rule. The Runge-Kutta method with four steps is consistent

w_1	w_2	w_3	w_4	α_2	α_3	α_4	β_{21}	β_{32}	β_{43}
$\frac{1}{6}$	$\frac{1}{3}$	$\frac{1}{3}$	$\frac{1}{6}$	$\frac{1}{2}$	$\frac{1}{2}$	1	$\frac{1}{2}$	$\frac{1}{2}$	1

Table 3.1.: weights and coefficients from Simpson's one-third-rule

up to fifth order in time $\mathcal{O}(dt^5)$ [PTVF92] and is used to approximate a time-dependent coefficient's evolution in the following.

3.3. Box-Muller algorithm

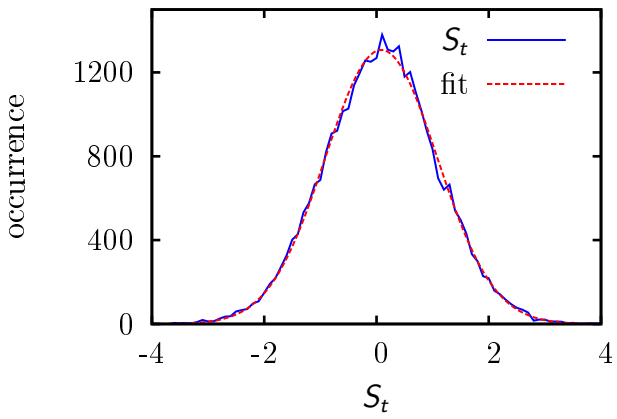

Figure 3.3.: Gaussian distributed random numbers generated with a Box-Muller algorithm. A Gaussian fit is approximated adequately.

Uniform random numbers were generated with a pseudo-random number generator returning an initial seed constructed by a thread-safe function using CPU-time. Gaussian distributed random numbers were achieved

utilising a Box-Muller algorithm as illustrated in figure 3.3 on the facing page.

$$S_1 = (-2 \ln X_1)^{1/2} \cos(2\pi X_2)$$
$$S_2 = (-2 \ln X_1)^{1/2} \sin(2\pi X_2)$$

Two uniform random numbers $X_{1,2}$ are used to generate two Gaussian distributed ones $S_{1,2}$ (following [BM58]). Those numbers are not perfectly independent, but figure 3.3 on the preceding page illustrates a sufficient approximation to a Gaussian distribution, as far as a deterministic computer is able to achieve (see also appendix A on page 89).

3.4. Kinetic Monte-Carlo wave function

A quantum system's time-evolution influenced by a bath is calculated in a reduced density matrix representation, usually. Here, a stochastic wave function can be utilised. The Kinetic Monte-Carlo (KMC) algorithm is a method to derive solutions to a stochastic Schrödinger equation, although not strictly norm conserving [MCD93]. The evolution of a system shall be represented by a linear combination of eigenstates of $\widehat{H}_0$. The resulting wave function is used to generate an averaged reduced density operator of the system. Starting from the identical initial wave function the outcome of different Monte-Carlo runs, indexing α, is diverse. But a stochastic wave function summed over N Monte-Carlo runs

$$\overline{\rho}(t) = \frac{1}{N} \sum_{\alpha=1}^{N} |\psi_\alpha(t)\rangle\langle\psi_\alpha(t)| \tag{3.4.1}$$

describes the averaged reduced density operator of the system $\overline{\rho}(t)$. The expectation value of any system operator $\widehat{A}$ is

$$Tr_S\{\widehat{A}\,\overline{\rho}(t)\} = \frac{1}{N} \sum_{\alpha=1}^{N} \langle\psi_\alpha(t)|\widehat{A}|\psi_\alpha(t)\rangle \tag{3.4.2}$$

In this equation Tr_S denotes the trace over the system's degrees of freedom (compare section 2.5.2 on page 31). Thus a system operator's mean can be calculated as accurately as in a reduced density matrix scheme, and even more efficient if the ensemble size N is optimised [MM99b].

A quantum system has different possibilities to interact with its environment. When the system is initially given by

$$|\psi_\alpha(t)\rangle = \sum_n c_n^\alpha(t)|n\rangle \tag{3.4.3}$$

with time-dependent complex numbers c_n^α and eigenstates $|n\rangle$ of $\widehat{H}_0$, the

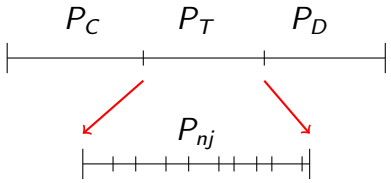

Figure 3.4.: Probabilities of the three major processes: dephasing (P_D), transition (P_T) or coherent propagation (P_C). The transition probability is subdivided into probability segments for every up- or downward transition.

idea is to decompose a time-step propagation into three different processes with different probabilities of occurrence:

- elastic collision probability $P_D = \gamma dt$ (dephasing)
- inelastic collision probability $P_T(t) = \sum_n \Gamma_n |c_n^\alpha(t)|^2 dt$ (transitions)
- coherent propagation probability $P_C(t) = 1 - P_T(t) - P_D$.

Here, $\Gamma_n = \sum_{j \neq n} k_{nj}$ is the escape rate from $|n\rangle$, while k_{nj} are transition rates and γ is a dephasing rate (compare equation (2.5.26)). At the very end of this work the rates for down-jump transitions and dephasing events will be selected, yet the up-jump rate is calculated from thermal equilibrium conditions (compare eq. (2.4.4)). An elastic or inelastic event can occur

in a time interval dt, during which a bath or reservoir is taking influence on a system. Additionally, there is a distinct probability of leaving the propagation coherent. If a uniform random number X_t falls into one of the segments (P_C, P_D, P_T) with $P_D + P_T(t) + P_C(t) = 1$, the corresponding propagation scheme is chosen:

- Dephasing propagation

$$|\psi_\alpha^D(t+dt)\rangle = \sum_n c_n^\alpha(t) e^{-i\delta_n^\alpha} |n\rangle \tag{3.4.4}$$

  with a random phase δ_n^α for each run and individual state

- Transitional propagation

$$|\psi_\alpha^T(t+dt)\rangle = c_n^\alpha(t) \frac{|j\rangle}{\sqrt{|c_n^\alpha(t)|^2}} \tag{3.4.5}$$

- Coherent propagation

$$|\psi_\alpha^C(t+dt)\rangle = \frac{1}{\sqrt{P_C(t)}} \sum_n c_n^\alpha(t) e^{-i\varepsilon_n dt} e^{\frac{-\Gamma_n dt}{2}} e^{\frac{-\gamma dt}{2}} |n\rangle \tag{3.4.6}$$

  where $P_C(t) = \sum_n |c_n^\alpha(t)|^2 e^{-(\Gamma_n+\gamma)dt}$ is the normalising factor

In case of a dephasing event, each phase of a coefficient $c_n^\alpha(t)$ in a run is shifted by different random phases $\delta_n^\alpha \in [0; 2\pi]$, possessing values between zero and a full cycle. The population of a state remains untouched by an elastic event. When a jump occurs, probabilities for a run $P_T(t) = \sum_n P_{nj}$ are distinguished into upward $j = n+1$ and downward $j = n-1$ next-neighbour transitions. Which transition is performed in particular, is determined from the segment within $P_T(t)$ in which the random number has fallen $P_{nj} = k_{nj} |c_n(t)|^2 dt$, as depicted in figure 3.4. The coherence of the final wave function is destroyed and the system resides in a single eigenstate of $\widehat{H}_0$. If a coherent evolution is to be performed, will say, the uniform random number falls into a time-dependent segment $P_C(t)$, the run propagates not only with its energy eigenvalue, but already takes the amount of dephasing runs involving transitions into account.

Justification

Following equation (3.4.1) the yield density operator is

$$\begin{aligned}\overline{\rho}(t+dt) &= \frac{1}{N}\sum_{\alpha=1}^{N}|\psi_\alpha(t+dt)\rangle\langle\psi_\alpha(t+dt)| \\ &= \frac{1}{N}\Big\{\sum_{\alpha=1}^{N_T}|\psi_\alpha^T(t+dt)\rangle\langle\psi_\alpha^T(t+dt)| \\ &+ \sum_{\alpha=1}^{N_C}|\psi_\alpha^C(t+dt)\rangle\langle\psi_\alpha^C(t+dt)| \\ &+ \sum_{\alpha=1}^{N_D}|\psi_\alpha^D(t+dt)\rangle\langle\psi_\alpha^D(t+dt)|\Big\} \\ &= \wp_T(t+dt)+\wp_C(t+dt)+\wp_D(t+dt), \end{aligned} \tag{3.4.7}$$

where the three components correspond to one of the earlier described processes. Since the probability of an inelastic transition process is given as $P_{nm}^{\alpha} = k_{nm}|c_n^{\alpha}(t)|^2 dt$, the density matrix for a transition process reads:

$$\wp_T(t+dt) = \frac{1}{N}\sum_{\alpha=1}^{N_T}\sum_{n,m}\frac{c_n^{\alpha,\star}(t)}{|c_n^{\alpha}(t)|}|m\rangle\frac{c_n^{\alpha}(t)}{|c_n^{\alpha}(t)|}\langle m| = \sum_{n,m}\frac{N_T}{N}|m\rangle\langle m|$$

with the ensemble average $\frac{N_T}{N} = \overline{P}_{nm} = dt\; k_{nm}\frac{1}{N_T}\sum_{\alpha=1}^{N_T}|c_n^{\alpha}(t)|^2$ follows

$$\begin{aligned} &= dt\sum_{n,m}k_{nm}\frac{1}{N_T}\sum_{\alpha=1}^{N_T}|c_n^{\alpha}(t)|^2|m\rangle\langle m| \\ &= dt\sum_{n,m}k_{nm}\overline{\rho}_{nn}(t)|m\rangle\langle m| \end{aligned} \tag{3.4.8}$$

This equation (3.4.8) is the transition contribution to the averaged density matrix. The dephasing contribution reads

$$\begin{aligned}\wp_D(t+dt) &= \frac{1}{N}\sum_{\alpha=1}^{N_D}\sum_{n,m}|m\rangle\langle n|c_n^{\alpha,\star}(t)c_m^{\alpha}(t)e^{-i(\delta_m^{\alpha}(t)-\delta_n^{\alpha}(t))} \\ &= \gamma dt\sum_{n,m}|m\rangle\langle n|c_n^{\alpha,\star}(t)c_m^{\alpha}(t)f_{nm} \\ &= \gamma dt\sum_{n,m}\overline{\rho}_{nm}(t)f_{nm} \end{aligned} \tag{3.4.9}$$

with the dephasing probability $\frac{N_D}{N} = P_D = dt\,\gamma$ and introducing a phase function $f_{nm} = \frac{N_D}{N}\sum_{\alpha=1}^{N_D} e^{-i(\delta_m^{\alpha}(t)-\delta_n^{\alpha}(t))}$. Finally, the coherent contribution is:

$$\begin{aligned}\wp_C(t+dt) = \frac{1}{N}\sum_{\alpha=1}^{N_C}\sum_{n,m}\frac{|m\rangle\langle n|}{\sqrt{P_C(t)}}c_n^{\alpha,\star}(t)c_m^{\alpha}(t) \\ e^{-i(\varepsilon_m-\varepsilon_n)dt}e^{-\frac{i}{2}(\Gamma_m-\Gamma_n)dt}e^{-\gamma dt}\end{aligned} \tag{3.4.10}$$

with the norm conserving function $P_C(t) \equiv 1 - dt\sum_n \Gamma_n|c_n^{\alpha}(t)|^2 - \gamma dt$. Thus, the contribution $\wp_C(t+dt)$ can be further simplified to

$$\begin{aligned}&= \sum_{n,m}|m\rangle\langle n|\overline{\rho}_{nm}(t) - idt\sum_{n,m}|m\rangle\langle n|(\varepsilon_m-\varepsilon_n)\overline{\rho}_{nm}(t) \\ &- dt\sum_{n,m}|m\rangle\langle n|\left(\frac{\Gamma_m-\Gamma_n}{2}+\gamma\right)\overline{\rho}_{nm}(t)\end{aligned} \tag{3.4.11}$$

Assembling all constitutions, one derives

$$\begin{aligned}\wp(t+dt) &= \wp_T(t+dt)+\wp_C(t+dt)+\wp_D(t+dt) \\ &= dt\sum_{n,m}k_{nm}\overline{\rho}_{nn}(t)|m\rangle\langle m| \\ &+ \sum_{n,m}|m\rangle\langle n|\overline{\rho}_{nm}(t) - idt\sum_{n,m}|m\rangle\langle n|(\varepsilon_m-\varepsilon_n)\overline{\rho}_{nm}(t) \\ &- dt\sum_{n,m}|m\rangle\langle n|\left(\frac{\Gamma_m-\Gamma_n}{2}+\gamma\right)\overline{\rho}_{nm}(t) \\ &+ \gamma dt\sum_{n,m}\overline{\rho}_{nm}(t)f_{nm}\end{aligned} \tag{3.4.12}$$

Examining the diagonal elements of the averaged density matrix

$$\begin{aligned}\langle \ell|\wp(t+dt)|\ell\rangle &= \overline{\rho}_{\ell\ell}(t+dt) \\ &= \overline{\rho}_{\ell\ell}(t) - dt\,\Gamma_\ell\,\overline{\rho}_{\ell\ell}(t) + dt\sum_n k_{n\ell}\overline{\rho}_{nn}(t)\end{aligned} \tag{3.4.13}$$

remains, which is equivalent to equation (2.5.27). The off-diagonal elements read

$$\begin{aligned}\langle m|\wp(t+dt)|n\rangle = \overline{\rho}_{mn}(t+dt) \\ = \overline{\rho}_{mn}(t) - idt(\varepsilon_m - \varepsilon_n)\overline{\rho}_{mn}(t) \\ - dt\left(\frac{\Gamma_m - \Gamma_n}{2} + \gamma\right)\overline{\rho}_{mn}(t) \\ + \gamma dt\overline{\rho}_{mn}(t) f_{mn}.\end{aligned} \tag{3.4.14}$$

With the simplification $\gamma_{mn} = \gamma(1 - f_{mn})$, this satisfies equation (2.5.26) and the KMC-method is proved to be equivalent to the reduced density matrix equations.

Implementation of KMC

The density matrix can be represented by a stochastic wave function and those wave functions can be decomposed into eigenfunctions of the Hamiltonian with time-dependent coefficients. An expansion into a spectral representation leads to a matrix for these coefficient rates

$$i\frac{d}{dt}c^\alpha_{1n}(t) = \varepsilon_{1n}c^\alpha_{1n}(t) + \widehat{W}(t)\sum_m \langle\chi_{1n}|\chi_{0m}\rangle\, c^\alpha_{0m}(t) \tag{3.4.15}$$

where $\widehat{W}(t)$ is a time dependent perturbation and $\langle\chi_{1n}|\chi_{0m}\rangle$ denotes the overlap matrix, consisting of factors introduced in equation (2.3.6). Obviously electronic ground and excited states are coupled by the interaction $\widehat{W}(t)$. This first order differential equation can be approximated with the fourth order Runge-Kutta method from section 3.2 on page 43,

while the control field entering the time-dependent perturbation in coherent runs has been calculated without any influence of the reservoir, i.e. for an isolated system, performing a full excitation from $|1\rangle \leftarrow |0\rangle$.

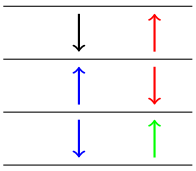

Figure 3.5.: Next-neighbour jumps scheme

A reservoir's influence relies on two processes, elastic or inelastic collisions, determined by their probabilities. For a transition the vibrational level's population $|c_n^\alpha(t)|^2$ is included in the probability calculation and a next neighbour jump is carried out (see figure 3.5). A vibrational state may depopulate into two neighbouring levels so to speak, why transition rates k_{nm} and k_{mn} can be simplified to an up- $k_n^\uparrow$ and downward $k_n^\downarrow$ jump rate from state $|n\rangle$. A uniform random number X_t decides which process is going to take place within a time step of a run, by falling into a probability segment P_C, P_T or P_D, as described earlier.

If a dephasing event takes place, the coefficient obtains a phase shift, if a jump occurs, all other levels are expunged. For simplicity, dephasing rates $\gamma_{mn} = \gamma$ equal $k_n^\downarrow$ in our simulations. In a coherent case the coefficient is propagated with its eigenenergy and is perturbed via the overlap matrix by the interaction with another electronic state within a Runge-Kutta scheme. Additionally, a norm conserving step is carried out, removing the influence of the damping terms by dephasing and jumps in the stochastic wave function.

Thus, one run is calculated independently for the whole duration, before the summation of the stochastic wave function to an averaged density operator is realised. Observables of interest are determined from the average over time-dependent coefficients from *all* runs (ensemble size N) according to equation (3.4.2). In order to gain less numeric wall time, the calculations are performed on different cores of a computing node simultaneously. For a grid size $M = 1024$ and an ensemble of $N = 1000$ runs a factor four

improvement of calculating time is achieved compared to a split-operator Fourier transform scheme. This method is applied to excitation processes in the sodium dimer in chapter 5 on page 57.

4. Phenol-Argon complex

In this section a method is presented, where the dynamics of a wave function is disturbed by a damping term containing potential energy curves. In a previous publication [WKS+10], the site-switching dynamics of argon

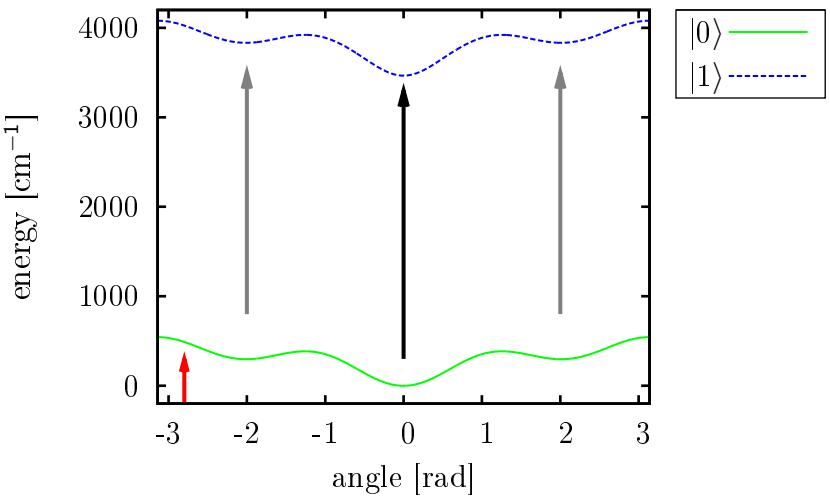

Figure 4.1.: Model electronic states of phenol-Ar along a reaction angle q: In the lower left corner is the pump pulse indicated (red). The excitation of the probe pulses is resonant at the π-binding site (grey) or the H-binding site (black arrow).

in a cationic phenol$^+$-Ar$_n$ potential is examined, a recently accepted phenomenon for acidic aromatic molecules interacting with non-polar solvents. There are two binding sites for argon in a phenol-Ar complex, hydrogen

bonding to the acidic OH-group and van-der-Waals bonding to the highly polarisable π-electron system of the aromatic ring. Since spectroscopic experiments have shown that the H-bonded isomer is a global and the π-bonded isomer only a less stable local minimum [KBCV$^+$09], figure 4.1 on the preceding page shows model potential curves along a reaction coordinate q. The angle is chosen as parameter, hence the mass is replaced by an effective rotational constant B_{eff}. A simple damping term as in equation (2.5.6) is used to force relaxation of the wave function into potential minima. The dissipative part $\widehat{Q}_n = \frac{\gamma}{2} V_n(q)$ incorporates into the Hamiltonian

$$\widehat{H}_n = -B_{eff} \frac{d^2}{dq^2} + V_n - i\widehat{Q}_n. \tag{4.0.1}$$

A Gaussian wave function is taken initially and different pump-pulses populate the potential surface V_0 at energetic values measured here in inverse centimetre[1]. The rotational constant determines the period of an unperturbed bound-state motion. Minima at different angles represent the hydrophilic H- or hydrophobic π-binding site. As seen in figure 4.2, a below-barrier excitation ($350\,\mathrm{cm}^{-1}$) is performed and the wave packet's angular mean is positioned in a local minimum. If an energetic potential barrier is exceeded ($400\,\mathrm{cm}^{-1}$), the wave packet is able to delocalise over the full coordinate range. The third alternative is to place the wave packet by a pump on a local maximum (barrier) ($380\,\mathrm{cm}^{-1}$), whereas it is split apart, consequently. The angular expectation value $\langle q \rangle_t$ gains components from a bifurcated wave function and tends to lower angles.

The wave packet has to be damped in a minimum, while relaxation is steered the larger the damping constant γ is chosen and an above-barrier excitation yields to an earlier damping into a minimum of the potential curve. The algorithm relies on two single parameters B_{eff} and γ to predict propagation in this model system. A third value can be used to compare results of the dynamics to an experiment, using a pump-probe laser ex-

[1] an inverse centimetre $1\,\mathrm{cm}^{-1} \simeq 12.4\,\mathrm{meV}$

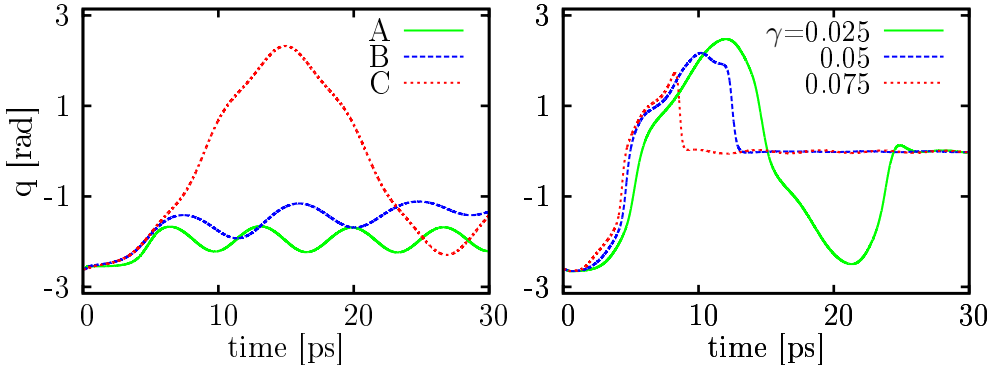

Figure 4.2.: Angular expectation value $\langle q \rangle_t$ after excitation: frequencies of $350\,\mathrm{cm}^{-1}$ (A), $380\,\mathrm{cm}^{-1}$ (B) and $400\,\mathrm{cm}^{-1}$ (C) without dissipation (left) and a pump with $430\,\mathrm{cm}^{-1}$ different damping constants γ (right)

citation scheme on the site-switching dynamics of argon within a cationic phenol-Ar complex, the delay time between the two ultrashort laser pulses. Because now, a laser tuned to the energetic difference between V_0 and V_1 at one of both binding-sites can selectively probe the time-dependence of the binding situation. In doing so, the transient spectroscopic signals for different delay times between pump- and probe-pulse are in excellent agreement with the model system (see [WKS+10]). This simple dissipative ansatz shown here, allows to interpret experimental data, already. But an even more sophisticated model shall offer clues about perturbations during a laser excitation.

5. Sodium dimer

In this chapter we regard the interaction of Na_2 molecules with laser control fields, in detail, a one photon excitation from the electronic ground state $|0\rangle$ ($X^1\Sigma_g^+$) to the excited state $|1\rangle$ ($A^1\Sigma_u^+$). This parallel transition

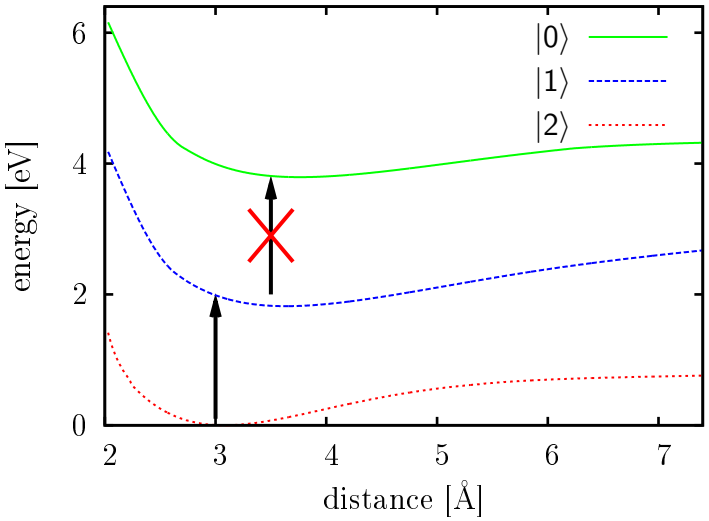

Figure 5.1.: Electronic states of the sodium dimer: $X^1\Sigma_g^+$,$A^1\Sigma_u^+$ and $2^1\Pi_g$ are denoted by $|0\rangle$, $|1\rangle$ and $|2\rangle$, respectively. A selective transition from $|1\rangle \leftarrow |0\rangle$ thereby excluding the transition $|2\rangle \leftarrow |1\rangle$ is illustrated.

is energetically comparable ($\lambda = 620\,\mathrm{nm}$ correlates to $\Delta\varepsilon = 1.818\,\mathrm{eV}$) to the separation between the first and second excited state ($2^1\Pi_g$), which is a perpendicular transition $|2\rangle \leftarrow |1\rangle$. While a two-photon excitation could populate state $|2\rangle$, here it is shown how to suppress the two-photon excitation by a control field which populates state $|1\rangle$ exclusively (see Fig. 5.1).

The adiabatic potential curves of the sodium dimer are taken from literature [KH78] [GM85] [TJS83] and sampled to a numeric grid with a cubic spline routine. The coupling strength is determined by the modulus of the respective transition dipole moment ($\widehat{\mu}_{01} = \widehat{\mu}_{10} = 9.14\,\mathrm{D}$ and $\widehat{\mu}_{12} = \widehat{\mu}_{21} = 3.65\,\mathrm{D}$ [KRH83]).

5.1. Applied local control

As discussed in section 2.4 on page 24 a system can be excited with a femtosecond-shaped laser pulse in a way completely populating the first excited state $|1\rangle$, although the energetic gap between $|1\rangle$ and $|2\rangle$ is resonant as well [BEMG92]. Figure 5.2 displays such a modelled LCT field with

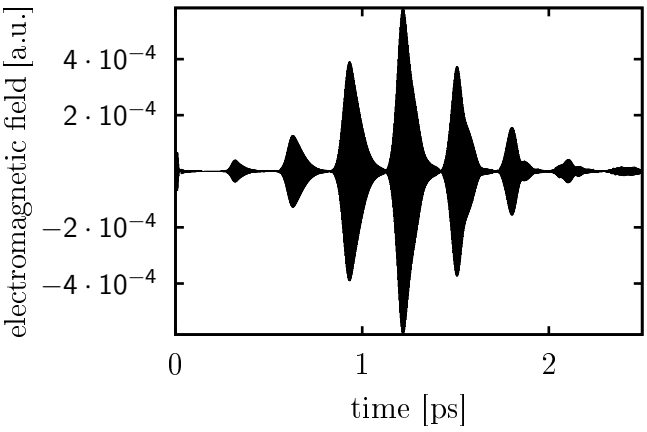

Figure 5.2.: A LCT field fulfilling the prior described selective excitation of state $|1\rangle$. This control field re-enters all further considerations on the influence of the surrounding.

sub-pulses separated by a motion of approximately 300 fs, which is the period of a vibronic wave packet in the first excited state. The modulation frequency in these pulses is proportional to the energetic gap $\Delta\varepsilon$ between the electronic states. An initial population is achieved by a seed pulse of

very low intensity, preceding the actual control field of the form

$$E_{seed}(t) = E_S \, e^{-\beta(t-t_0)^2} \cos(\omega t) \tag{5.1.1}$$

with parameter $\beta = 4\log(2)t_0^{-2}$ and the seed amplitude $E_S = 7 \cdot 10^{-5}$ a.u. ($4{\cdot}10^7 \frac{\mathrm{V}}{\mathrm{m}}$) with a 30 fs Gaussian envelope centred at time $t_0 = 10$ fs [GEE05]. The control field is the result of the adaption to the dynamics of the system. By no means at all, are Rabi-like oscillations (compare figure 2.5 on page 27) involved, because of the electromagnetic field's low amplitude ($E_0 = 7 \cdot 10^{-4}$ a.u.). An excitation can only take place from the ground to the first excited state, when there is an overlap between the wave packets in these electronic states, because the overlap determines the electric field (see eq. (2.4.2)). Considering orientation and the properties of the LCT

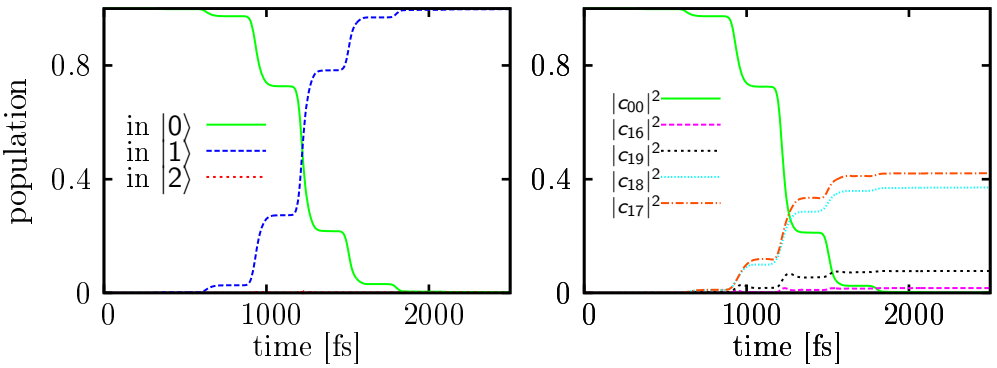

Figure 5.3.: An excitation or population transfer accomplished by a LCT field. On the left hand side the total population is shown and the right hand panel illustrates the transfer in different vibrational levels, represented by their populations $|c_{1n}|^2$. Also shown is the population of the initial state $|c_{00}|^2$.

field (see section 2.1 on page 11), a complete and selective transfer is guaranteed into the first excited state depicted in figure 5.3. There is a monotonic increase of the first excited electronic state population connected to the associated monotonic decrease of the ground state. The population varies in steps at times the sub-pulses arrive. The control field affects the vibrational level's populations $|c_{1n}|^2$ in the first excited state of the sodium

dimer molecule. The eigenfunction overlapping the most with the ground state eigenfunction are favoured, owing to the largest Franck-Condon factor. During one period of the excited state oscillatory motion, the wave packet leaves the Franck-Condon region and the generated field goes to zero. A negligible population in $|2\rangle$ causes the field not to completely disappear during that time. The wave packet traverses the minimum of the potential curve twice and is reflected in between at the outer potential wall. Returning to the overlap region, the field increases again and thus is able to transfer population to the first excited state another time, and so forth. By the time the population transfer achieves nearly 100%, the control field assumes marginal values, which is at 2.5 to 3 ps, in our case. In the following the field generated here (see Fig. 5.2 on page 58) will enter into the field-matter interaction. There is no intention, to adapt the field to any particular influence of the environment, or even optimise the control field, but examine the efficiency of the perturbed control.

5.2. Interaction with a reservoir

The system-bath approach is able to describe dissipation processes, but is computationally demanding, in general. Dissipation is based on collisions. Elastic or inelastic impacts result in a dephasing or an energy transfer, respectively. We want to investigate the question of laser control of our model system brought into an environment consisting of other particles. A so called open quantum system as described in section 2.5 on page 29 is considered in what follows. Three differing approaches will be discussed, within which the last one is most promising.

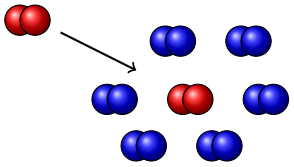

Figure 5.4.: Scheme of a dimer in an environment

5.2.1. Stochastic Hamiltonian

A stochastic Hamiltonian term was regarded by Singh and Rost [SR07] in order to simulate fluctuations:

$$\widehat{h}_s(R,t) = \sqrt{\frac{2D}{dt}} S_t \widehat{R} \tag{5.2.1}$$

The fluctuation amplitude reads D. The above distance and time-dependent term is coupled linearly to the molecule, that means, it modifies the potential energy surfaces. A Gaussian distributed random number S_t with zero mean generated for every time step by a Box-Muller algorithm is used, with values from $[-\pi, \pi]$ (section 3.3 on page 44). At first the stochastic Hamiltonian $\widehat{h}_s$ is added in the diagonal elements of the system-Hamiltonian:

$$i\frac{\partial}{\partial t}\begin{pmatrix}\psi_0(t)\\ \psi_1(t)\\ \psi_2(t)\end{pmatrix} = \begin{pmatrix}\widehat{T}+\widehat{V}_0+\widehat{h}_s & \widehat{W}_{01} & 0\\ \widehat{W}_{10} & \widehat{T}+\widehat{V}_1+\widehat{h}_s & \widehat{W}_{12}\\ 0 & \widehat{W}_{21} & \widehat{T}+\widehat{V}_2+\widehat{h}_s\end{pmatrix}\begin{pmatrix}\psi_0(t)\\ \psi_1(t)\\ \psi_2(t)\end{pmatrix} \tag{5.2.2}$$

Since rotational degrees of freedom are not considered here, simply the vibrational Hamiltonian is perturbed. Additional perturbations in the interaction term are discussed below. The probability of a random collision to occur in this picture is found to be $P_{dt} = 2DR^2dt$. This comes from the modified probability density $|\widehat{U}_S(dt)\psi(t)|^2 \sim |\psi(t)|^2 + P_{dt}S_t^2|\psi(t)|^2$, which contains a random term of size P_{dt} additionally. The fluctuation amplitude D includes all parameters as the scattering cross section ζ of the involved particles, their number density η and temperature T. Figure 5.5 illustrates the fluctuation-free (left) and perturbed situation (centre) of potential curves $V_n(R)$ in a sodium dimer molecule. Surfaces are perturbed with $D = 10^{-4}$ a.u., a time step of $dt = 0.1$ fs and random numbers $S_t = \pm 1$. In what follows, the efficiency of the control process, as discussed in section 5.1, under noise is investigated.

That a fluctuation-free LCT field – without the stochastic Hamiltonian – is already in the position to represent dissipative effects, is shown on the

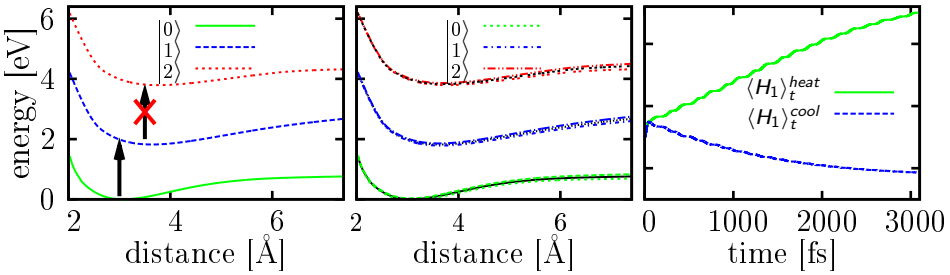

Figure 5.5.: Potential energy curves of the sodium dimer depicted fluctuation-free on the left. Perturbations cause fluctuations in the potentials and thus disturb the electronic excitation induced by the control field (centre [KME09]). In the right panel a dissipation after excitation is illustrated, heating up or cooling down the dimer.

right hand side to clarify that vibrational motion is accelerated, if an external electric field acts in the same direction as the system's momentum. By defining the sign of the parameter $\lambda = \pm 10^{-5}$, a control field $E(t) \approx \lambda \langle \widehat{p} \rangle$ (see eq. (2.4.3)) will heat up (+) or cool down (-) the system, representing the influence of the surrounding reservoir, shown in figure 5.5 right hand side. The energy expectation values $\langle \psi_1(t)|H_1|\psi_1(t)\rangle(t) = \langle H_1 \rangle_t$ in the first excited electronic state are depicted here, exhibiting an in- or decrease which is associated with an energy exchange with the bath (being the electromagnetic field).

Figure 5.6 illustrates how the fluctuation parameter D of the stochastic Hamiltonian affects the population transfer by the control field in time. Representing a sufficient ensemble size to cope with statistics, succeeding figures demonstrate the average over $N = 500$ runs. The population transfer into the excited electronic state decreases with increasing D. For the unperturbed case ($D = 0$ a.u.) the population reaches about 100% in $|1\rangle$, whereas a fluctuation amplitude of $D = 10^{-3}$ a.u. results in 20% excited state population. The energy expectation value behaves alike. When no perturbation is present, $\langle H_1 \rangle_t$ reaches 1.81 eV in 2 ps and for $D = 10^{-5}$ a.u. the maximal energy is reached after 1.5 ps at approximately 1.4 eV. The

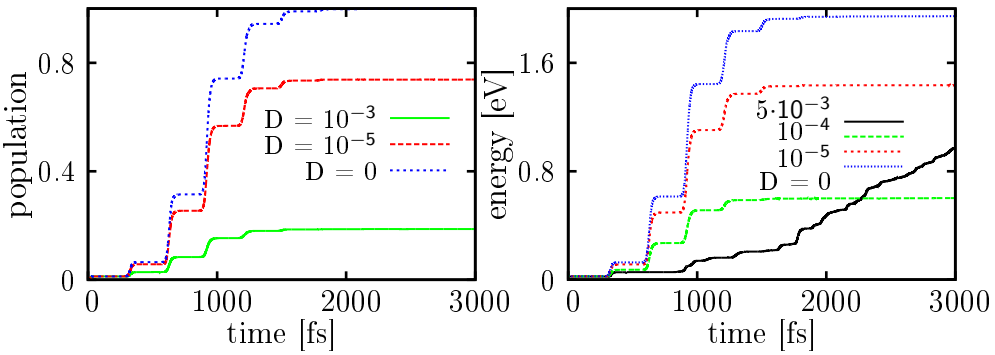

Figure 5.6.: Population after LCT excitation (left) and energy expectation value $\langle \widehat{H}_1 \rangle_t$ (right) decrease with growing fluctuation parameter D (in atomic units) in the stochastic Hamiltonian.

stepwise population transfer takes place at the same time as the rise in energy. For noises larger $D = 10^{-3}$ a.u., the energy expectation value grows although the control field is of negligible amplitude. The left graph in

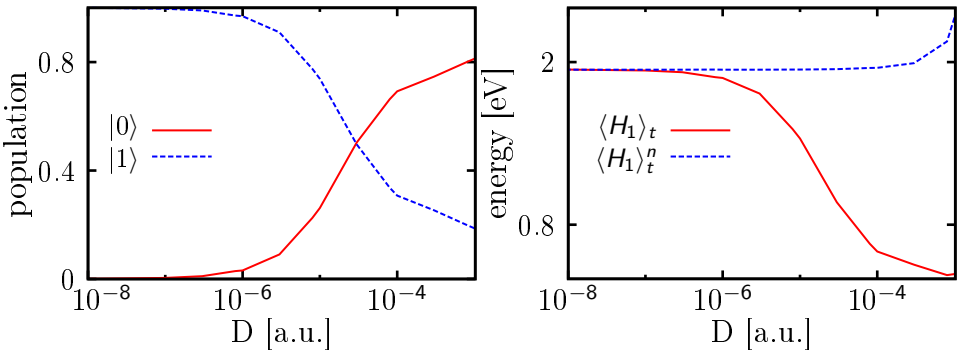

Figure 5.7.: Final excited and ground state population versus perturbation parameter D (left). The normalised energy expectation value of the excited state diverges (right).

figure 5.7 shows the decrease of the final populations on the perturbation parameter D. These functions are calculated after the control field stops interacting with the system at about 3.2 ps. We conclude that the control field is state selective at negligible perturbation amplitudes, because populations in $|0\rangle$ and $|1\rangle$ add up to approximately 100%. Our numeri-

cal simulation shows that the second excited state does not exceed 0.2% for $D = 5 \cdot 10^{-5}$ a.u.. The population transfer is monotonically decreasing as a function of D. As does the energy expectation value. However, the normalised energy expectation value

$$\langle \widehat{H}_1 \rangle_t^n = \frac{\langle \psi_1(t) | \widehat{H}_1 | \psi_1(t) \rangle}{\langle \psi_1(t) | \psi_1(t) \rangle} \tag{5.2.3}$$

which measures the mean energy of the excited state wave packet independent of its population, experiences an increase.

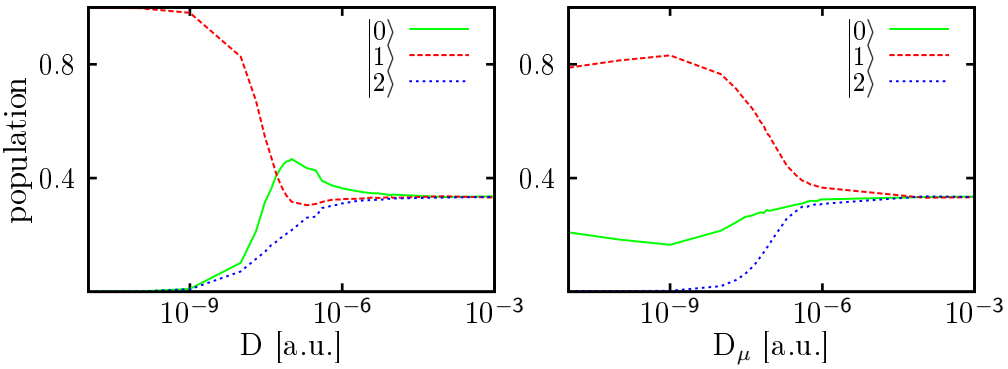

Figure 5.8.: The final population versus the fluctuation parameter D in a three-state scheme. In the right panel, the perturbation parameter modifying the diagonal parts of the Hamiltonian is set to a value of $D_{diag} = 10^{-5}$a.u., whereas the off-diagonal fluctuation amplitude D_μ is varied.

The diagrams in figure 5.8 depict results obtained by incorporation of a stochastic term in the diagonal parts of the Hamiltonian and additionally the off-diagonal part. This includes the possibility that not only the vibrational Hamiltonian, but also the dipole coupling is influenced by fluctuations. To study this effect in detail, the diagonal part of the fluctuation is included with a constant amplitude $D_{diag} = 10^{-5}$a.u., and the off-diagonal part D_μ was varied. This reflects the collisions perturbing the electronic wave functions which enter into the transition dipole moments. Figure 5.8 shows that equipartition between all states is reached for large values of D_μ.

Because $\widehat{h}_s$ appears in the off-diagonal elements of the Hamiltonian of figure 5.8, the fluctuations themselves transfer population. In the right panel a population transfer of about 80% is the maximum, since the constant D_{diag} in the vibrational Hamiltonian constraints the population transfer. Figure 5.9 illustrates that the time-dependence of the coordinate and momentum expectation values behave as anticipated. For a low fluctuation amplitude range of about $D = 10^{-6}$, simulations yield results [KME09], in agreement with the dissipative influence of the surrounding, but the energy expectation value is not conserved for larger fluctuations. Taking the stochastic part of the short time propagator $\widehat{U}_S(dt) = e^{-i\widehat{h}_s dt}$ into account,

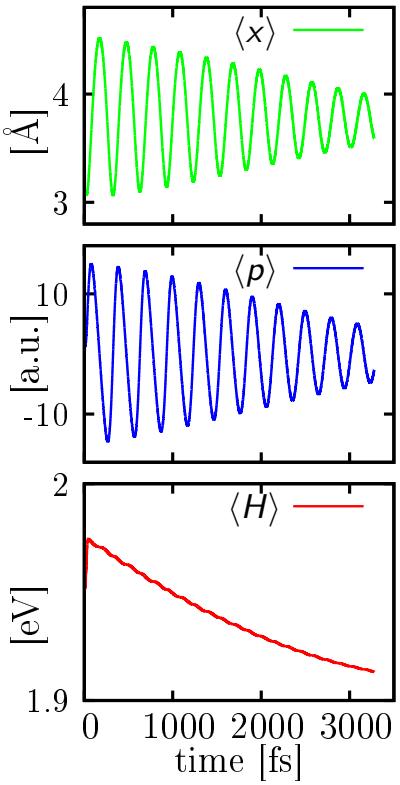

Figure 5.9: First excited state expectation values: the bond length shows oscillatory behaviour as well as the momentum, while the energy relaxes, if the fluctuation amplitude is small $D = 10^{-6}$.

the exponential expanded to first order reads

$$\begin{aligned}\langle e^{-i\widehat{h}_s dt}\psi_0(t)|\widehat{H}_0|e^{-i\widehat{h}_s dt}\psi_0(t)\rangle &= \langle\psi_0(t)|\widehat{H}_0|\psi_0(t)\rangle \\ &\quad - i\sqrt{2Ddt}S_t\langle\psi_0(t)|\left[\widehat{R},\widehat{H}_0\right]|\psi_0(t)\rangle \\ &\quad + DdtS_t^2\langle\widehat{R}\psi_0(t)|\widehat{H}_0|\widehat{R}\psi_0(t)\rangle \\ &= \langle\widehat{H}_0\rangle_t + \frac{Ddt}{m}S_t^2 - \frac{\sqrt{2Ddt}}{m}\langle\widehat{p}_0\rangle_t S_t \quad (5.2.4)\end{aligned}$$

in which m is the molecule's reduced mass and $\widehat{p}$ the momentum operator. While the term $\propto S_t$ alternates signum with the sign of the random number, the term $\propto S_t^2$ is always positive and explains the trend of the normalised energy expectation value in figure 5.7 on page 63. Thus this ansatz results in an overall dissipation of energy into the perturbed system and is set aside.

5.2.2. Dissipation in a harmonic oscillator

A more sophisticated ansatz to describe dissipation is presented by Mølmer et al. [MCD93], in that the system's propagation is described with

$$\frac{d}{dt}\rho = i[\rho,\widehat{H}_S] + \Lambda(\rho) \quad (5.2.5)$$

as was already shown in (2.5.25). The rate of a reduced density matrix calculates from its commutator with the system Hamiltonian and a relaxation superoperator $\Lambda(\rho)$, which is given as

$$\Lambda(\rho) = \gamma\, a\rho a^\dagger - \frac{\gamma}{2}(a^\dagger a\rho + \rho a^\dagger a). \quad (5.2.6)$$

γ^{-1} corresponds to a lifetime and $\widehat{a},\widehat{a}^\dagger$ are harmonic oscillator lowering and raising operator, respectively (compare (2.5.8)).

A harmonic oscillator is an approximation to treat vibrational motion in molecules. A system's Hamiltonian of a single harmonic oscillator reads

$$\widehat{H}_S = \omega(\widehat{a}^\dagger\widehat{a} + \frac{1}{2}) \quad (5.2.7)$$

with $\widehat{a}$ and $\widehat{a}^\dagger$ are defined as

$$\widehat{a}^\dagger = \frac{1}{\sqrt{2}}(\widehat{Q} + i\widehat{P}) \tag{5.2.8}$$

$$\widehat{a} = \frac{1}{\sqrt{2}}(\widehat{Q} - i\widehat{P}) \tag{5.2.9}$$

Here, $\widehat{P}$ and $\widehat{Q}$ denote canonical space and momentum operators. A har-

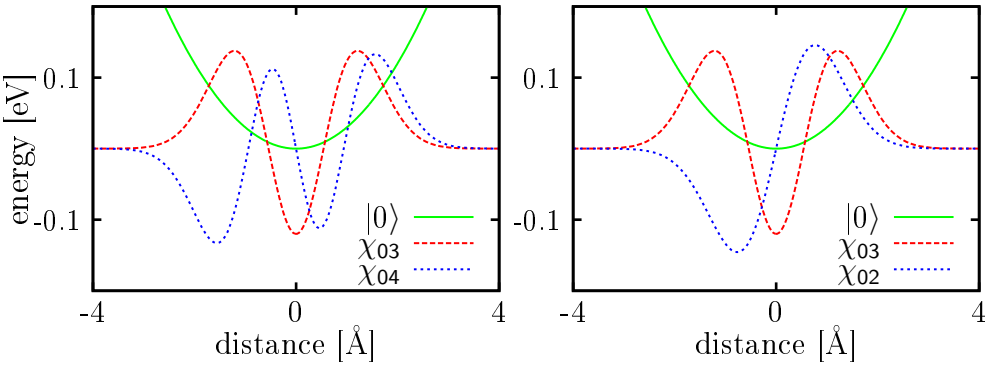

Figure 5.10.: Case I: A harmonic oscillator around zero distance, where the third eigenstate is raised (left) or lowered (right) in one propagation step.

monic oscillator potential curve, $V_n(x) = \frac{1}{2}m\omega^2x^2$ adapted to the ground state of the sodium dimer with the reduced mass m and $\omega = 0.01418\,\text{eV}$, centred around zero (case I) is illustrated in figure 5.10. The raising operator $\widehat{a}^\dagger$ rises population from an eigenstate to the next higher one, while $\widehat{a}$ lowers it. In the numerical simulation they evolve the initial to the final wave function as $\psi_f = \widehat{a}^\dagger\psi_i$ and $\psi_f = \widehat{a}\psi_i$, respectively. As initial wave function ψ_i the eigenfunction χ_{03} is taken. The left panel shows an up-jump from eigenfunction χ_{03} to χ_{04} and the right one the down-jump $|0,2\rangle \leftarrow |0,3\rangle$, whereas the first index belongs to the electronic ground state $|0\rangle$ and the second one is the particular vibrational quantum number. Equally spaced vibrational energy levels are directly specified via eigenvalues of the number operator $\widehat{N} = \widehat{a}^\dagger\widehat{a}$ in $\varepsilon_n = \omega(n + \frac{1}{2})$, in which n denotes the vibrational quantum number. If a quantum of energy sized $\Delta\varepsilon = \omega$ is absorbed, the next vibrational mode is populated. This scheme

is working as well for a dislocated harmonic oscillator, but as a realistic potential curve is approached (an-harmonic case II in Fig. 5.11), it brings up misleading results. A Gedanken an-harmonicity of size $\widehat{W} = \varsigma\omega\widehat{Q}^3$ leads to shifted energy eigenvalues and lowered energetic gaps (see appendix A on page 94):

$$\varepsilon_n - \varepsilon_{n-1} = \omega(1 - \frac{15}{2}\varsigma^2 n) \tag{5.2.10}$$

Eigenvalues are not equidistant in a non-harmonic oscillator potential. They are lowered because ς^2 is positive. Though, most molecular potentials can be approximated within a harmonic oscillator model system in the vicinity of their stable equilibrium distance, the second case (Fig. 5.11) does not generate correct eigenfunctions in utilising lowering and raising operators. While the creation operator produces a new wave function with

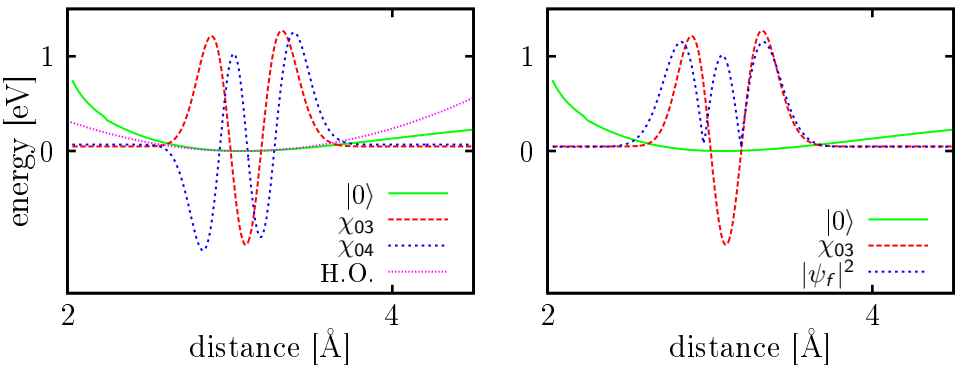

Figure 5.11.: Case II: A non-harmonic oscillator (sodium dimer) with a minimum at 3.06 Å distance, where the third eigenstate is raised (left). The harmonic approximation to the potential is included for comparison. The lowering process is depicted in one propagation step (right). The wave function as well as the energy do not behave as expected.

the correct nodal structure, the annihilation counterpart does not lower to χ_{02}, but provides a complex-valued wave function ψ_f, which has the same amount of nodes (right panel). The resulting wave function is neither orthogonal to χ_{03}, nor do their energetic means differ from each other significantly. Since energetic levels get closer in an an-harmonic potential

curve, lowering and raising operator introduced for a harmonic potential are not in the position to characterise our model system adequately. The description of system-bath effects using harmonic raising and lowering operators is questionable.

5.2.3. Coefficient time-evolution

The right hand panel of figure 5.3 on page 59 shows the effect of a control field and its correlation to vibrational dynamics in transferring a population into vibrational eigenstates, efficiently. The portion of the wave

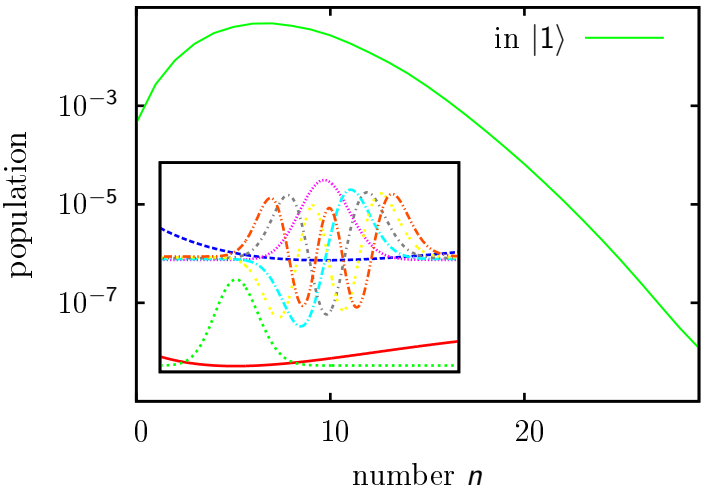

Figure 5.12.: The population $|c_{1n}|^2$ in vibrational levels of the excited state is illustrated. Eigenstates around $n \approx 7$ are mainly populated by the control field, a sample of eigenfunctions is embedded (see Fig. 2.3).

packet in each vibrational level is described by $|c_{mn}|^2$. The unperturbed case – no influences of the surrounding on the transfer process – is illustrated in figure 5.12, the modulus squared of a coefficient on a logarithmic scale versus quantum number is displayed. Eigenfunctions of the excited electronic state (small sample) overlapping the most with the vibrational ground level of the electronic ground state, become more populated by the

control field. Maximum contribution comes from the states around $n \approx 7$, possessing the largest Franck-Condon factors. These wave functions – like strings in the picture of a spatially confined resonator – obtain more nodes $(n-1)$ the larger the vibrational quantum number (n) is and hence more wave elevations (n). These wave peaks approach the boundary represented by the potential curve for larger quantum numbers and have then a larger overlap area. A basis set of 30 eigenfunctions in all electronic states is taken into account in what follows to describe the excited state vibrational wave packet in a sufficient manner.

Time-step examination

The creation of a control field and the population transfer depend crucially on the time step. Figure 5.13 shows on the left the unperturbed (no en-

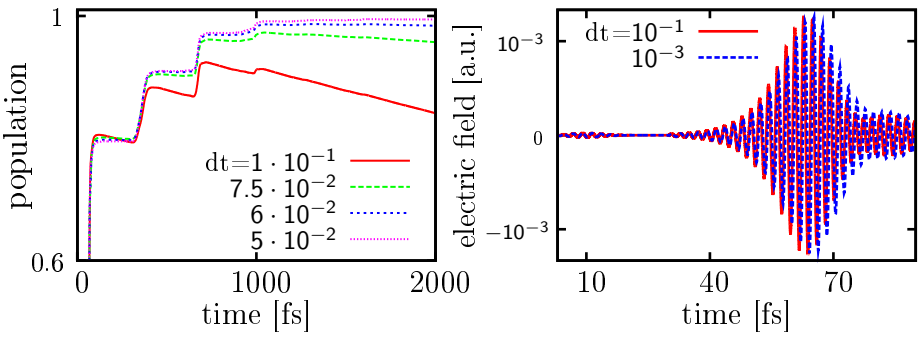

Figure 5.13.: The time increment dt affects a population transfer (left). A sampling of one sub-pulse of the electric field reveals a different shape with a different dt (right).

vironment included) population transfer affected by the size of the time step in a Runge-Kutta propagation scheme. The population in the excited state $(\sum_n |c_{1n}(t)|^2)$ reaches almost 100% after 2 ps for the smallest time step $dt = 5 \cdot 10^{-2}$ fs. The larger an increment, the more the respective curve deviates. Even during interim times as the control field is more or less zero, the population in the excited state declines. This illustrates the

necessity to choose a small timestep in order to reach convergent results. In what follows, dt is fixed to a value of $5 \cdot 10^{-2}$ fs.

On the right of figure 5.13 a control field is depicted, which is constructed with a time step of $1\,as$ (blue) and of $100\,as$ (red). In *Local Control Theory* the field is generated in every time step from the dynamics of the system. This means, to be able to respond on molecular dynamics in the right moment, the field changes its shape instantaneously. A field sampled with a 100 larger time-step is already too purely sampled, to keep up with the right phase condition of the particular wave packet and has to adapt during its generation. This explains the difference in curves shown here.

5.3. Stochastic Schrödinger equation

A tool to describe a system of a canonical ensemble by wave functions instead of density operators is introduced in section 3.4 on page 45 gaining grid size M-dimensional solutions instead of $M \times M$. A single time propagation to describe a system's evolution is not sufficient and an acceptable ensemble size – a mean over repeated runs – is to be taken. Preliminary considerations will guide to our final findings in section 5.3.1 on page 78.

Ensemble size consideration

To ensure good statistics the number of different runs must be sufficiently large. In figure 5.14 is displayed, how the ensemble size affects the result of a control field driven excitation versus time. Three different collision rates are illustrated, but since a more specific consideration of perturbation will follow later, it is only necessary to understand the term 'rate' in the graph here, as a value for a fluctuation influencing the transfer process. From left to right the ensemble size increases from 10 to 1000 runs. Numerically, those are the iterations a program is executed with the same prerequisite – in all but random numbers – and an average is taken over

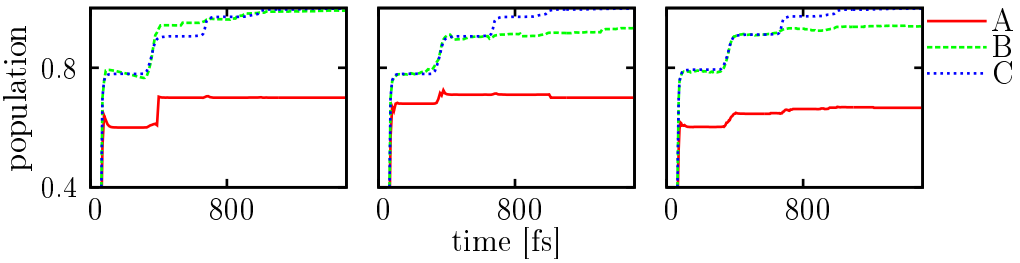

Figure 5.14.: Optimising the ensemble size from 10 (left), 100 (centre) to 1000 runs (right), while different rates $10^{-1}\,\mathrm{fs}^{-1}$ (A), $10^{-3}\,\mathrm{fs}^{-1}$ (B) and $10^{-5}\,\mathrm{fs}^{-1}$ (C) influence the excitation. The more runs are summed up, the smoother the curves become and reflect the demanded monotonic increase in the first excited state.

the sum of all runs. Few iterations produce steps in, for example, populations versus time. A larger ensemble reflects less discontinuities, but still a non-monotonic increase of excited state population, which is demanded by the field. Eventually, the biggest ensemble shows the smoothest curves incorporating less effects of those various fluctuations on population transfer processes and a steady increase as well. All fluctuations covered later in this section will more or less constrain evenness of a function, hence an ensemble size of $N = 1000$ runs is chosen in the numerical examples shown below.

Dissipation processes

Earlier discussed (see Fig. 5.5 on page 62), the choice of a mathematical parameter λ in the generation of a control field is capable to influence, whether dissipation is heating or cooling the system. From now on the ratio $k_n^{\uparrow}/k_n^{\downarrow}$ of inelastic collision rates will perform this task. Considered in figure 5.15 is an isolated single electronic state $|0\rangle$ with an initial population, equally distributed in three of the 15 vibrational eigenstates χ_{04}, χ_{05}, χ_{06}. We examine two cases separately. The probability for a jump is either non-zero $P_{mn} = k_{mn}|c_n(t)|^2 dt \neq 0$ for an up- $(m = n + 1)$ or downward case $(m = n - 1)$ in a next-neighbour scheme. In other words,

once $k_n^{\uparrow} = 0$ while $k_n^{\downarrow} \neq 0$ and vice versa. The rates are chosen $0.2\,\mathrm{fs}^{-1}$

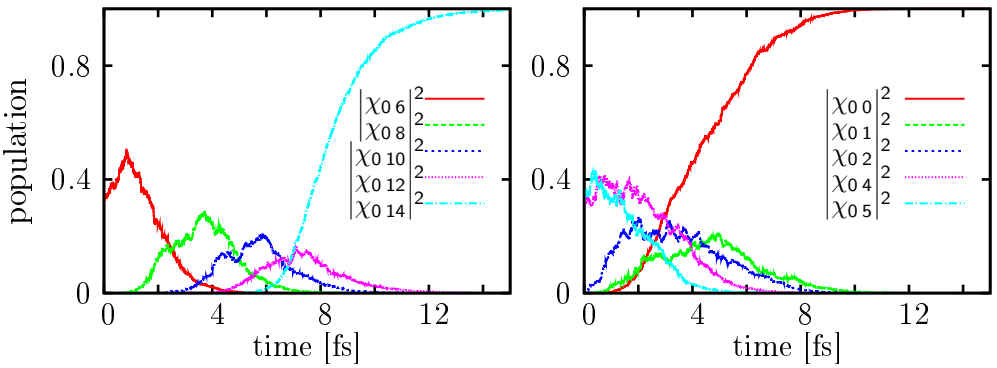

Figure 5.15.: Up- (left) or down-jump (right) preferred dissipation in the arbitrary occupied electronic ground state $|0\rangle$ consisting of 15 eigenfunctions. On the left hand side the topmost vibrational mode, on the right hand side the ground state is fully populated in the end.

while transitions and coherent propagation can occur. If up-jumps are preferred, one ends up with the complete population inside the highest included state. Up-jumps represent a collision, where energy is absorbed by the system and when those occur, the intermediate states gain population temporarily. If energy is taken out of the system via inelastic collisions in a down-jump scheme, just the ground state remains. Thus one speaks of an energy relaxation in a downward and energy absorption in an upward case. The transitions used here are next-neighbour jumps, so no level is left out in shifting in down- or upward direction. All intermediate levels are populated transiently, before the sum of all populations of one electronic state reaches an outer level completely. For further considerations the transition probabilities P_{nm} will not arbitrarily be set zero, rather than depend on temperature of the surrounding reservoir, of course.

Temperature analysis

The influence of temperature on collision rates is described in Eq. (2.4.4), where the collision rate ratio is weighted with a Boltzmann factor [MM99a].

The down-jump rate will be preferred as the balance condition is $k_{mn} =$

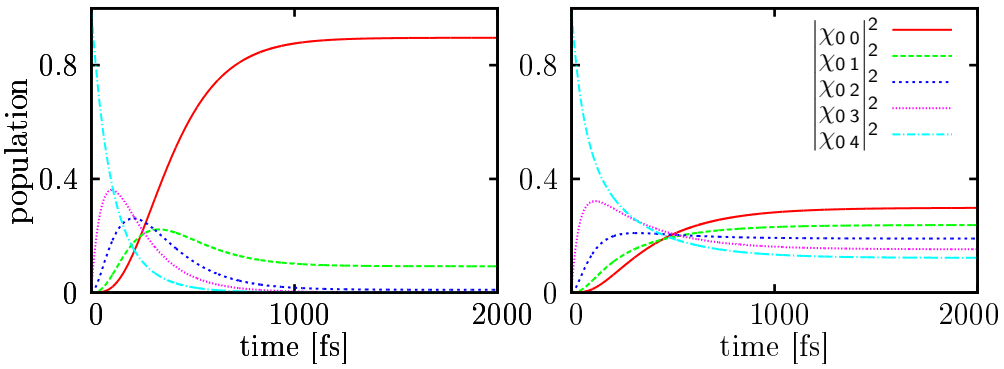

Figure 5.16.: Influence of temperature on damping: vibrational state population $|c_n(t)|^2$ as a function of time with an environment at $100\,\mathrm{K}$ (left) and $10^3\,\mathrm{K}$ (right). After $2\,\mathrm{ps}$ populations are Boltzmann distributed.

$k_{nm}\, e^{\frac{E_m - E_n}{k_B T}}$, while the temperature is non-zero and finite. The rate is $k_{nm} = 2 \cdot 10^{-3}\,\mathrm{fs}^{-1}$ for transitions, while the majority of runs propagates coherently. This means, for a low temperature the relaxation into the lowest vibrational level is preferred, however not completely since $T > 0\,\mathrm{K}$. At a higher temperature the system tends to an equipartition of the populations of several vibrational modes as anticipated (compare figure 5.16). So, interaction with the hot reservoir conducts an energy placing into the model system. From an arbitrary initial population the eigenstates become Boltzmann distributed after equilibrium is reached. In agreement with Maxwell-Boltzmann statistics this incorporation of temperature reflects correct numerical procedures.

Fluctuations

As presented in section 3.4 on page 45, there are three different propagation schemes for the dynamics of a wave packet. In figure 5.17 it is pictured how three evenly populated vibrational eigenstates in the electronic state $|1\rangle$ evolve in time if a coherent scheme alone or other schemes are applied. For the calculations in each scheme the wave packet expands as in eq. (3.4.3)

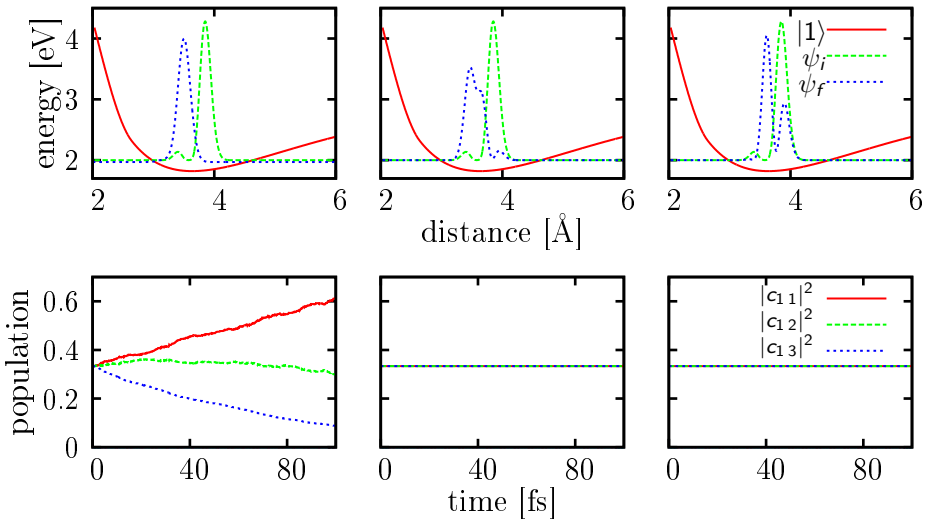

Figure 5.17.: Dynamics for a pure coherent (right), a dephasing (centre) and a low temperature down-jump transition propagation scheme (left): upper panels show an initial wave packet equally composed of three eigenfunctions and the final one after a propagation of 100 fs. The lower panels illustrate the populations of these eigenstates in the first excited state versus time.

in coefficients and 1000 individual runs are propagated. The $c_n^\alpha(t+dt)$ assemble into new wave functions in the elastic $\psi_\alpha^D(t+dt)$, inelastic $\psi_\alpha^T(t+dt)$ or coherent $\psi_\alpha^C(t+dt)$ scheme (see eqns. (3.4.4) - (3.4.6)).

A shift of population to the ground state demonstrates the down-jump transition scheme at a temperature $T = 100\,\mathrm{K}$ with maximal 20% transition runs. The final wave packet resembles the ground state (χ_{10}). This is a low temperature case of inelastic collisions and represents a transfer of vibrational energy into the reservoir. Moreover there is a dephasing scheme illustrated. These elastic events leave the populations invariant, while the relative phases between vibrational modes differ. Thus, the wave packet changes its position erratically on the spatial grid. Populations $|c_n(t)|^2$ do not change for a pure coherent propagation as well, but the relative phase correlations between $\Im(c_n(t))$ and $\Re(c_n(t))$ are affected. The wave packet oscillates around the potential curve's minimum, because complex and real

part of a coefficient c_n substitute, so its squared absolute value remains constant. Following examinations incorporate these collision schemes into a consideration of several electronic states.

Treatment of several electronic states

Electronic states, exchanging population via a LCT field, have to be treated specially in a KMC scheme, because the wave packets need to be normalised with respect to the total wave function. Once a control field has populated

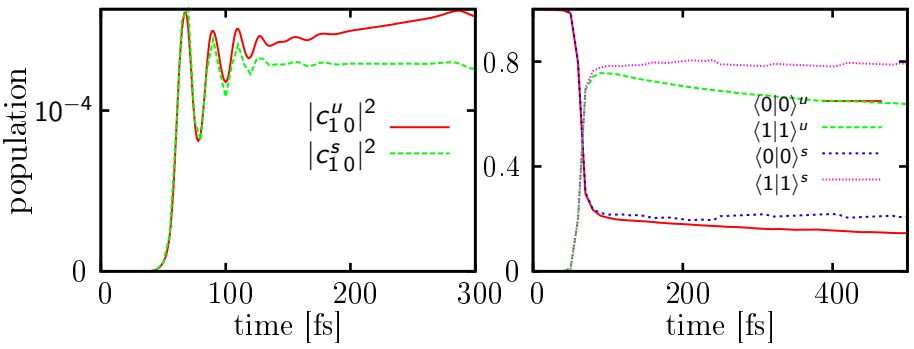

Figure 5.18.: Electronic states separation: damping into outermost levels, if the excitation into an electronic state is treated (s)eparately or (u)nseparated from the dissipation (left), results in a decrease of the norm (right).

a vibrational mode in the excited state, as illustrated in figure 5.18, the coherent propagation has to be normalised onto this population before fluctuations are performed. So, there has to be a strict separation of the interaction process with the control field and the dissipation by the reservoir.

The coherent propagation of c_n in a Runge-Kutta procedure has to be executed twice, first with the interaction $\widehat{W}(t)$ and with a phase $\propto \frac{-\Gamma_n-\gamma}{2}$, secondly. Otherwise a normalisation with the factor $P_C^{-1/2}$ after each time-step leads to a loss of norm. Given that $P_C = 1 - P_D - \sum_m P_{nm}$, in which $P_{nm} \propto |c_n(t)|^2$, the current populations appear in the normalisation, which manifests by a damping of intermediate vibrational level population into

both outer ones in the next neighbour scheme. I.e., the more population is in an eigenstate the larger is the probability of a transition. Since all intermediate levels can de-populate in two directions except the outer ones, those become favoured. In separating electronic states, two new outer levels are gained – the lowest of the excited state and the highest of the ground state, which possess no neighbours in one direction.

Figure 5.18 depicts the difference in usage during a control field excitation. A coherent propagation without any collisions is shown, where the population of the excited state is once normalised on just itself or onto the total wave function in both electronic states. This curve reflects a counter-intuitive damping into the lowest vibrational level by a *coherent* propagation as long as no transition occurs with a normalising factor $P_C^{-1/2}$ from equation (3.4.6), following [MM99b]. The control field is switched off after $150\,\mathrm{fs}$ in the population versus time illustration on the right and the loss of norm can be seen. An average over few runs was taken here, only to clarify the need of a sufficient ensemble size. Before we move on from preliminary considerations to the results, we settle the matter of parametrisation in the next paragraph.

Dependence of collision rate on temperature and number density

In our model we use collision rates and temperature as parameters, which are proportional to each other via the number density η. Using the estimation that the mean velocity of an ideal gas particle $\overline{v} = \sqrt{\frac{8k_B T}{m\pi}}$ [CC70] divided by the mean free path $\lambda_{free} = \frac{1}{\eta\,\zeta\,N_L}$results in the collision rate

$$k_n^{\downarrow} = \eta\,\zeta\,N_L\sqrt{\frac{8k_B\,T}{m\pi}}. \tag{5.3.1}$$

Here occurs a scattering cross-section $\zeta = (3.06\,\text{Å})^2$ of the order of a sodium dimer diameter squared, its reduced mass $m = 22.99\,\mathrm{u}$ (atomic weights) and the Loschmidt constant $N_L \approx 2.6 \cdot 10^{23}\,\mathrm{m}^{-3}$. Figure 5.19 shows the time-dependent population transfer parametrised with either the tempera-

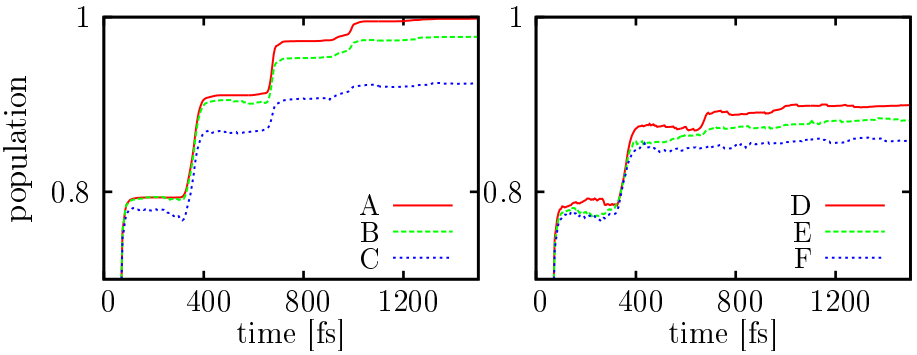

Figure 5.19.: Population in the excited state versus time for a fix rate = $10^{-4}\mathrm{fs}^{-1}$ but different temperatures, 10^3 K (A), 10^6 K (B) and 10^7 K (C), so the number density varies (left). The parametrisation of number density for 0.5 (D), 0.7 (E) and 1 amagat (F) for a fix temperature $T = 10^8$ K for the purpose of illustration varies the rate (right).

ture at a fix rate or via number density at a fix temperature. Excessive values are chosen to sharpen the view on variations. The population transfer influenced by a constant collision rate is scanned over a couple of temperatures, which means the higher the temperature the less population will be transferred because of fluctuations of the bath. When the number density is varied, more particles in a certain volume disturb an excitation as they interfere with the system. We decided to parametrise collision rates and temperature in further considerations.

5.3.1. Results for the dynamics with fluctuations

In what follows, we concentrate on the ground and first excited state in our theoretical treatment and want to apply all the former considerations to the sodium dimer. Consequently, all propagation schemes described before are shown in figure 5.20, where a combined population transfer into $|1\rangle$ versus time influenced by different collision rates is depicted. The above mentioned rate is integrated in inelastic downward transitions ($k_n^{\downarrow}$) – with a Boltzman factor also in up-jumps ($k_n^{\uparrow}$) – as well as in elastic collisions

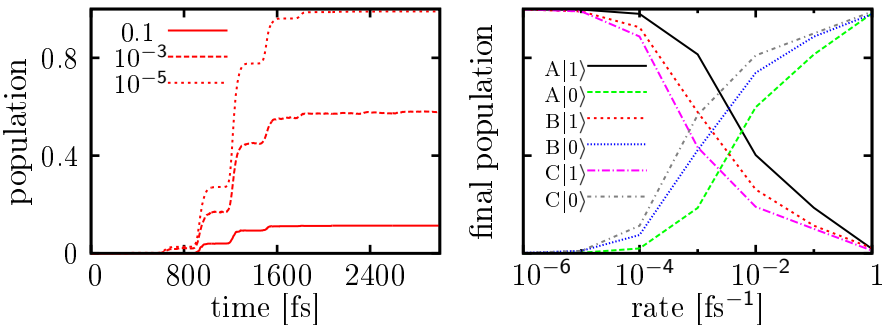

Figure 5.20.: Time-evolution of populations in $|1\rangle$: the decrease of rates results in less collisions and so a better control at room temperature (left). Final population vs. rate: shown are 1 K (A), room temperature (B) and 10^3 K (C). The higher the temperature is, the more sodium dimers collide with other particles, and the control field excitation is perturbed at lower rates (right).

(γ), eventually. So the specified rate enters maximally with a factor three for high temperatures when $k_n^{\uparrow} \approx \gamma = k_n^{\downarrow}$. A larger effect of a denser bath prevents excitation, as expected. Also shown is the final population – after a complete control field cycle – versus the rate for three different temperatures. With a lower temperature a minor influence of the reservoir is anticipated. The population majority remains in the electronic ground state for rates larger than 10^{-2}fs^{-1}. For a temperature of 10^3 K this is already the case for collision rates of about 10^{-3}fs^{-1}. Expectation values for a 100 K bath, having a collision statistically every picosecond, are illustrated in figure 5.21. While the bond length $\langle x_0 \rangle$ in the electronic ground state remains at the equilibrium value, the excited state's spatial expectation value oscillates around its minimum and relaxes into the vibrational ground state. Although a damping takes place, the behaviour of a sodium dimer molecule coupled to a dissipative bath, is described adequately, because the energy expectation value $\langle H \rangle^n = \frac{\langle \psi | H | \psi \rangle}{\langle \psi | \psi \rangle}$ of neither the ground, nor excited electronic state differ from their initial values significantly. The normalised energy expectation value of this method does not

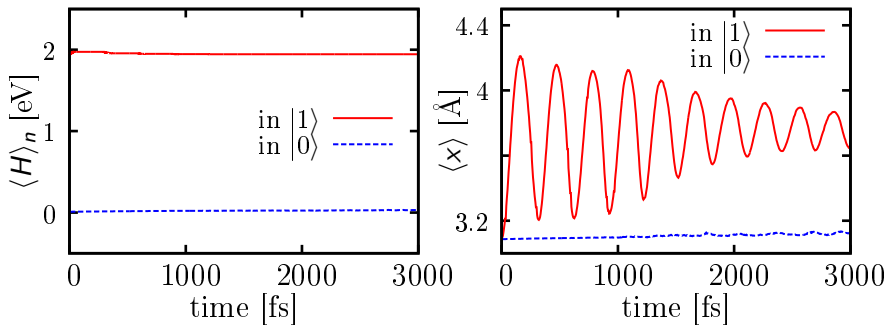

Figure 5.21.: Damping at a temperature of 100 K and a rate of $10^{-3}\,\mathrm{fs}^{-1}$: the energy expectation value (left) and the bond length (right) behave as anticipated, converging into minima of the potential curves.

grow exponentially as in the case of the stochastic Hamiltonian discussed earlier (in Fig. 5.7 on page 63). It approaches the value of 1.83 eV, which corresponds to the energy of the excited state's lowest vibrational level ε_{10}, according to the distribution in Fig. 5.16 on page 74. Energy expectation values obtained including the various events are shown in figure 5.23 at a

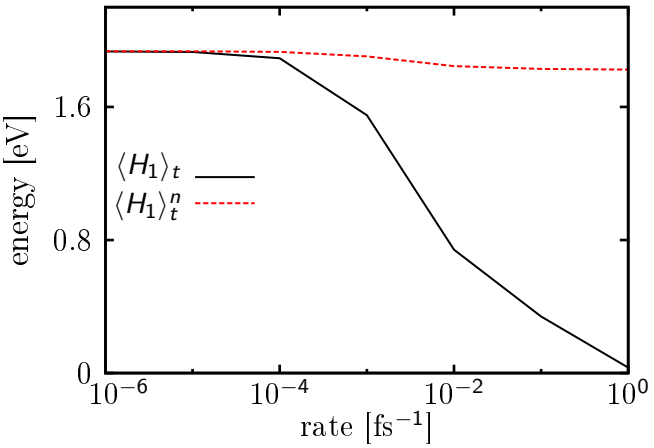

Figure 5.22.: Energy expectation values obtained with the KMC method in the excited state. One vanishes proportional its population, while the normalised approaches an energy close to ε_{10} at 100 K.

temperature of 100 K versus the rate. The impact of the single schemes, transition curves (T), elastic collisions (D), and also for all combined processes (A) are shown. The population transfer induced by a LCT field is carried out completely at low rates, but the higher collision rates and therefore the influence get, the lower the final excited state population is. The difference for low temperature curves is caused by stochastics – different random numbers. In an infinite ensemble they should look alike, in fact, rates of inelastic and elastic processes are in the same regime, since down-jump transition rates $k_n^{\downarrow}$ equal dephasing ones γ. All these rates are given as parameters in our scheme as $k_n^{\downarrow}$ and γ, while $k_n^{\uparrow}$ calculate from a Boltzmann distribution. As higher temperatures are reached, the upward-

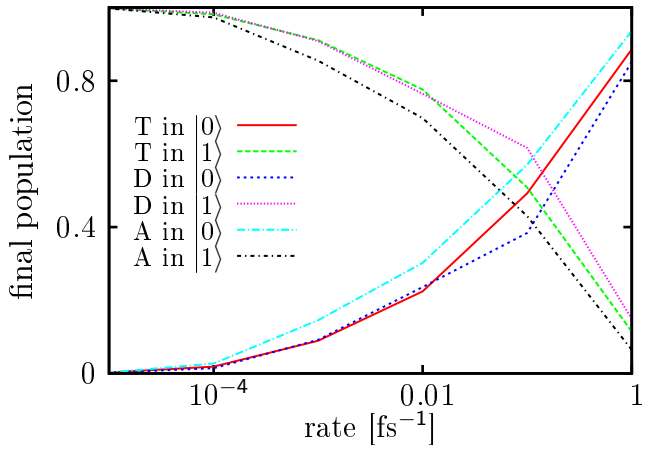

Figure 5.23.: Different schemes of collisions: the final population versus the rate in a transition (T), a dephasing (D) and an combined one (A).

jump rates $k_n^{\uparrow}$ grow and will double the effect of inelastic collisions, thus their influence perturbs the excitation in an earlier stage – at lower rates. Up to rates of about $10^{-4}\,\mathrm{fs}^{-1}$, where population is still selectively transferred into the first excited state, the outcome of the excitation is quasi untouched. Until rates exceed $3 \cdot 10^{-2}\,\mathrm{fs}^{-1}$ the minority of the population remains in the ground state, after that excitation is less efficient than 50%. The control field, initially generated to transfer a system into an excited

state without any coupling to a heat bath, loses efficiency. Insight into the influence of decoherence-processes on control is gained via electronic excitation of a sodium dimer molecule in contact with a reservoir.

6. Conclusion

In this thesis, the influence of an environment on molecules and, in particular, on the quantum control of such systems is investigated. Different approaches to describe system-bath dynamics are implemented and applied.

The inclusion of a dissipation term in the system Hamiltonian leads to energy loss and relaxation to the ground state. As a first application, the isomerisation reaction in an aromatic complex is treated. It is shown that this simple model is able to reproduce results of time-resolved spectroscopic measurements.

Next, the influence of noise is investigated. The incorporation of fluctuations reveals that energy is not conserved and coherences are destroyed. As an example, the quantum control of a population transfer in Na_2 is examined. The efficiency of control processes is studied in dependence on the strength of the noise and different system-bath couplings. Starting with the unperturbed system, Local Control Theory is applied to construct a field which selectively transfers population into a single excited electronic state. The coupling to the bath is then switched on to monitor the dependence of the coupling strength on the transfer efficiency.

The perturbation of the bath effects the Na_2 molecule in such a way that potential energy curves and transition dipole moments are distorted. An important result is that already elastic collisions lead to a substantial loss of control efficiency.

The most promising approach used in this thesis is the stochastic Schrödinger equation. It is equivalent to the commonly employed descriptions

of system-bath dynamics within the reduced density matrix formalism. It includes decoherences and dissipation caused by elastic and inelastic collisions. Our contribution is the incorporation of laser excitation into the kinetic Monte-Carlo scheme. Thus we are able to apply this stochastic approach to the quantum control of population transfer in the sodium dimer. Because within our description it is possible to separate pure dephasing, inelastic transitions, and coherent time-evolution, we can identify the relative influence of these processes on the control efficiency. This leads to a far more physical picture of the basic processes underlying the perturbations of an environment then what a reduced density matrix description can provide.

In utilising the stochastic wave function approach instead of the density matrix formalism, the computations are quite efficient. The stochastic Schrödinger equation is realised by N independent runs, where, in our case, an ensemble size of $N = 1000$ gives converged results. The efficiency of the laser control process is studied as a function of temperature and collision rates. A rise in temperature (or collision rate) reflects a stronger fluctuation and thus results in a less efficient transfer by the control field.

Though the Gaussian fluctuations used here do not strictly represent 'white'-noise, since a deterministic machine is not able to produce uncorrelated random numbers, an acceptable distribution is achieved by simple procedures. An improvement of the here applied algorithms would, for instance, include a more sophisticated sampling of the dephasing rates. Only one example of a control process is studied here and an application of the developed approach to other problems of quantum control is to be performed.

This thesis established a systematic approach to understand quantum control in the presence of an environment.

7. Zusammenfassung

In der vorliegenden Arbeit wird der Einfluss der Umgebung auf Moleküle und insbesondere der Quantenkontrolle solcher Systeme untersucht. Unterschiedliche Herangehensweisen, System-Bad-Kopplungen zu beschreiben, werden implementiert und angewendet.

Die Berücksichtigung eines Dissipationstermes im System-Hamiltonoperator führt zu Energieabgabe und Relaxation in den Grundzustand. Als eine erste Anwendung wird die Isomerisation eines aromatischen Komplexes behandelt. Anhand dieses einfachen Modells ist es möglich, Resultate zeitaufgelöster, spektroskopischer Messungen zu reproduzieren.

Weiterhin wird der Einfluss des Rauschens untersucht. Die Einführung von Fluktuationen führt dazu, dass Energie nicht erhalten bleibt und Kohärenz verloren geht. Als ein Beispiel dient hier die Quantenkontrolle eines Populationstransferprozesses im Na_2 Molekül. Die Effizienz eines Kontrollprozesses wird in Abhängigkeit der Rauschstärke und verschiedener System-Bad-Kopplungen untersucht. Ausgehend vom ungestörten System wird die Lokale Kontrolltheorie benutzt, um ein Feld, welches selektiv Population in einen einzigen, angeregten Zustand transferiert, zu konstruieren. Die Kopplung an das Bad wird daraufhin eingeschaltet, um die Abhängigkeit der Kopplungsstärke auf die Transfereffizienz zu charakterisieren.

Die Störung des Bades beeinflusst das Na_2-Molekül dahingehend, dass Potentialkurven und Übergangsdipolmomente verzerrt werden. Eine wichtige Erkenntnis ist, dass bereits elastische Stöße zu einem substantiellen Verlust der Kontrolleffizienz führen.

Die am meisten versprechende Methode, welche in dieser Arbeit Verwendung findet, ist die der stochastischen Schrödingergleichung. Sie ist der weitläufig gebräuchlichen Beschreibung von System-Bad-Wechselwirkungen innerhalb des Formalismus der reduzierten Dichtematrix gleichwertig. Dekohärenzen und Dissipationseffekte ausgelöst durch elastische und inelastische Stöße werden innerhalb der stochastischen Gleichungen separat berücksichtigt. Unser Beitrag ist die Einbindung der Laseranregung in das kinetische Monte-Carlo-Schema. Dies ermöglicht die Anwendung des stochastischen Ansatzes auf die Quantenkontrolle des Populationstransfers eines Natriumdimers. Da es innerhalb unserer Beschreibung möglich ist, reine Dephasierungen, inelastische Übergänge und kohärente Entwicklung in der Zeit zu beschreiben, können wir den relativen Einfluss jener Prozesse auf die Kontrolleffizienz identifizieren. Dies führt zu einer physikalischeren Beschreibung der zugrunde liegenden Prozesse, welche die Störungen der Umgebung bewirken, als sich aus einer reduzierten Dichtematrizendarstellung ergibt.

Durch Benutzung des stochastischen Wellenfunktionsansatzes anstelle des Dichtematrizenformalismus ergeben sich effiziente Berechnungen. Die stochastische Schrödingergleichung wird für N unabhängige Programmdurchläufe gelöst, wobei in unserem Fall eine Ensemblegröße von $N = 1000$ konvergente Resultate liefert. Die Wirksamkeit des Laserkontrollprozesses wird anhand von Temperatur und Stoßrate untersucht. Ein Anstieg der Temperatur (oder der Stoßrate) spiegelt höhere Fluktuationen wider und resultiert daher in einem weniger effizienten, von einem Kontrollfeld hervorgerufenen Transfer.

Obwohl die gaußverteilten Fluktuationen, welche hier benutzt werden, strenggenommen kein 'Weisses Rauschen' repräsentieren, da eine deterministische Rechenmaschine keine unkorrellierten Zufallszahlen generieren kann, wird dennoch eine akzeptable Verteilung aus einfachen Prozeduren erhalten. Eine Verbesserung der hier angewendeten Algorithmen würde zum Beispiel aus einer verfeinerten Implementierung der Dephasierungsrat-

en bestehen. Lediglich ein Beispiel eines Kontrollprozesses wird hier untersucht und die Anwendung der erarbeiteten Methodik auf andere Fragestellungen der Quantenkontrolle ist noch offen. Diese Dissertation stellt somit eine systematische Annäherung dar, um die Quantenkontrolle in Anwesenheit von Umgebungseinflüssen zu verstehen.

A. Appendix

A.1 Hartree atomic units

$\hbar, m_e, e = 1$ with Planck's constant by 2π, mass of an electron and elementary charge are unity [Mil93].

A.2 Prefices

femto $= 10^{-15}$, pico $= 10^{-12}$, nano $= 10^{-9}$, micro $= 10^{-6}$ and milli $= 10^{-3}$

A.3 Random numbers

Procedures to achieve uniform random numbers.

- random_number: GCC pseudo-random number generator
- random_seed: initial number for random_number
- gmtime: thread-safe function returns CPU-time as seed for random_seed

The χ^2-test of our *gnuplot* fit to the Gaussian random numbers revealed:

```
Iteration 6
WSSR        : 49082.4      delta(WSSR)/WSSR   : -6.57445e-08
delta(WSSR) : -0.00322689  limit for stopping : 1e-05
lambda   : 2.15451e-07
```

```
resultant parameter values
a               = 1307.71
b               = 0.0862288
c               = 1.40966
After 6 iterations the fit converged.
final sum of squares of residuals : 49082.4
rel. change during last iteration : -6.57445e-08
degrees of freedom    (FIT_NDF)                       : 78
rms of residuals      (FIT_STDFIT) = sqrt(WSSR/ndf)   : 25.0851
variance of residuals (reduced chisquare) = WSSR/ndf: 629.261
Final set of parameters            Asymptotic Standard Error
=======================            ==========================
a               = 1307.71          +/- 7.307        (0.5588%)
b               = 0.0862288        +/- 0.006433     (7.461%)
c               = 1.40966          +/- 0.009098     (0.6454%)
correlation matrix of the fit parameters:
                a      b      c
a                1.000
b                0.000  1.000
c               -0.577 -0.000  1.000
```

A.4 Expectation values

$$\begin{aligned}\frac{d\langle\widehat{A}\rangle}{dt} &= \frac{d}{dt}\langle\Psi|\widehat{A}|\Psi\rangle \\ &= \frac{\partial}{\partial t}(\langle\Psi|\widehat{A}|\Psi\rangle) + \left\langle\frac{\partial\widehat{A}}{\partial t}\right\rangle \\ &= \left\langle\frac{\partial\widehat{A}}{\partial t}\right\rangle + \langle\frac{\partial}{\partial t}\Psi|\widehat{A}|\Psi\rangle + \langle\Psi|\widehat{A}|\frac{\partial}{\partial t}\Psi\rangle\end{aligned}$$

with the time-dependent Schrödinger equation

$$
\begin{aligned}
&= \left\langle \frac{\partial \widehat{A}}{\partial t} \right\rangle + \langle i\widehat{H}\Psi|\widehat{A}|\Psi\rangle + \langle \Psi|\widehat{A}|-i\widehat{H}\Psi\rangle \\
&= \left\langle \frac{\partial \widehat{A}}{\partial t} \right\rangle + i\langle \Psi|\widehat{H}\widehat{A}|\Psi\rangle - i\langle \Psi|\widehat{A}\widehat{H}|\Psi\rangle \\
&= \left\langle \frac{\partial \widehat{A}}{\partial t} \right\rangle + i\langle \Psi|[\widehat{H},\widehat{A}]|\Psi\rangle
\end{aligned}
$$

A.5 Commutator

$$
\begin{aligned}
R\frac{\partial^2}{\partial R^2}\Psi - \frac{\partial^2}{\partial R^2}(R\Psi) &= R\frac{\partial^2\Psi}{\partial R^2} - \frac{\partial}{\partial R}\left(\frac{\partial R}{\partial R}\Psi + R\frac{\partial \Psi}{\partial R}\right) \\
&= R\Psi'' - (\Psi' + \Psi' + R\Psi'') \\
&= -2\Psi'
\end{aligned}
$$

A.6 Born-Oppenheimer approximation

Kinetic energy

$$
\widehat{T} = \sum_{n=1}^{N_n} \frac{1}{2M_n}\widehat{P}_n^2 + \frac{1}{2m_e}\sum_{\ell=1}^{N_e}\widehat{p}_\ell^2
$$

with M_n masses, $\widehat{P}_n$ momenta of the nuclei and $\widehat{p}_\ell$ momenta of the electrons, while the potential energy consists of scalar Coulomb-potentials as:

$$
\widehat{V}_e = \frac{1}{2}\sum_{j\neq\ell}^{N_e}\frac{e^2}{|r_j - r_\ell|}
$$

$$
\widehat{V}_n = \frac{1}{2}\sum_{n\neq m}^{N_n}\frac{Z_n Z_m e^2}{|R_n - R_m|}
$$

$$
\widehat{V}_{n-e} = -\sum_{n}^{N_n}\sum_{j}^{N_e}\frac{Z_n e^2}{|r_j - R_n|}
$$

Non-adiabatic kinetic coupling terms ($\widehat{K}'_{j\ell}(R), \widehat{K}''_{j\ell}(R)$) are neglected:

$$(\widehat{T}_{nuclei} + V_j(R))\chi_{jm}(R) + \sum_{\ell} \left(2\widehat{K}'_{j\ell}(R) + \widehat{K}''_{j\ell}(R)\right) \chi_{\ell n}(R) = \varepsilon_{jm}\chi_{jm}(R)$$

A.7 Condon-Approximation

$$\vec{\mu} = \sum_{\alpha} Z_\alpha \vec{R}_\alpha + \sum_{i}(-e)\vec{r}_i$$

in a spectral representation

$$|\Psi\rangle = |\chi_{jk}(\vec{R})\varphi_j(\vec{r}, \vec{R})\rangle$$

follows

$$\vec{\mu}_{jk\leftarrow mn} = \left\langle \chi_{mn}(\vec{R})\varphi_n(\vec{r}\right| |\vec{\mu}| \left|\chi_{jk}(\vec{R})\varphi_j(\vec{r}\right\rangle$$

where a dipole compound of electronic and nuclear part

$$\begin{aligned}
&= \left\langle \chi_{mn}(\vec{R})\varphi_n(\vec{r}, \vec{R})\right| \vec{\mu}_N(\vec{R}) \left|\chi_{jk}(\vec{R})\varphi_j(\vec{r}, \vec{R})\right\rangle \\
&+ \left\langle \chi_{mn}(\vec{R})\varphi_n(\vec{r}, \vec{R})\right| \vec{\mu}_e(\vec{r}) \left|\chi_{jk}(\vec{R})\varphi_j(\vec{r}, \vec{R})\right\rangle \\
&= \left\langle \chi_{mn}(\vec{R})\right| \vec{\mu}_N(\vec{R}) \overbrace{\left\langle \varphi_n(\vec{r}, \vec{R})\right| \varphi_j(\vec{r}, \vec{R})\right\rangle_r}^{\delta_{nj}} \left|\chi_{jk}(\vec{R})\right\rangle_R \\
&+ \underbrace{\left\langle \chi_{mn}(\vec{R})\right| \chi_{jk}(\vec{R})\left\rangle_R}_{\text{overlap factors}} \cdot \left\langle \varphi_n(\vec{r}, \vec{R})\right| \vec{\mu}_e(\vec{r}) \left|\varphi_j(\vec{r}, \vec{R})\right\rangle_r
\end{aligned}$$

The Condon-approximation neglects the R-dependence of φ_n, φ_j of the electronic dipole moment.

A.8 Energy and time in quantum mechanics

Time is nothing but a parameter in quantum mechanics and can not act as an operator. Starting with Heisenberg's equation

$$\Delta A \cdot \Delta B \geq \frac{1}{2}|\langle[\widehat{A}, \widehat{B}]\rangle|$$

the uncertainty between an arbitrary operator $\widehat{A}$ and the Hamiltonian as shown on page 90 reads

$$\Rightarrow \Delta\widehat{A} \cdot \Delta\widehat{H} \geq \frac{1}{2} \left| i\frac{d\langle\widehat{A}\rangle}{dt} - i\left\langle \frac{\partial\widehat{A}}{\partial t} \right\rangle \right|$$

in the Schrödinger picture no operator is time-dependent and the norm removes the imaginary unit

$$\Rightarrow \Delta\widehat{H} \cdot \frac{\Delta\widehat{A}}{\frac{d\langle\widehat{A}\rangle}{dt}} \geq \frac{1}{2}$$

the variance in the denominator reads

$$\Rightarrow \Delta\varepsilon \cdot \frac{\sqrt{(\widehat{A} - \langle\widehat{A}\rangle)^2}}{\frac{d}{dt}\langle\widehat{A}\rangle} \geq \frac{1}{2}$$

and units of energy times time remain on the left hand side. A pure dimensional analysis reveals that energy relates a time span in which a mean value changes.

A.9 Fourier grid method

A spatial grid of grid size M is divided in $M-1$ intervals

$$\Delta x = \frac{(x_{end} - x_0)}{(M-1)}.$$

Coordinates in momentum space are achieved by Fourier transformation with

$$\Leftrightarrow p_{max} < \frac{2\pi}{\Delta x}$$

where function values at p_{max} are excluded, since they overlap values at zero momentum. The maximal resolvable momentum is

$$p_{max} - \Delta p = (M-1)\Delta p =$$
$$\Leftrightarrow M\Delta p = p_{max}$$

why the momentum grid is of size M (without a value at p_{max}).

A.10 Anharmonicity

$$\begin{aligned}\widehat{W} &= \varsigma\omega\widehat{Q}^3 \quad \text{with} \quad \widehat{Q} = \frac{1}{\sqrt{2}}(\widehat{a}^\dagger + \widehat{a}) \quad \text{and} \quad [\widehat{N}, \widehat{a}] = -\widehat{a}, [\widehat{N}, \widehat{a}^\dagger] = \widehat{a}^\dagger \\ &= \frac{\varsigma\omega}{2^{3/2}}(\widehat{a}^\dagger + \widehat{a})^3 \\ &= \frac{\varsigma\omega}{2^{3/2}}\left((\widehat{a}^\dagger)^3 + \widehat{a}^3 + 3(\widehat{N}\widehat{a} + \widehat{a}) + 3\widehat{N}\widehat{a}^\dagger\right)\end{aligned}$$

evaluate for $|n-3\rangle$ to $|n+3\rangle$

$$\begin{aligned}W_{n-1,n} &= 3\varsigma(\frac{n}{2})^{3/2}\omega \\ W_{n+1,n} &= 3\varsigma(\frac{n+1}{2})^{3/2}\omega \\ W_{n-3,n} &= \varsigma(\frac{n(n-1)(n-2)}{8})^{1/2}\omega \\ W_{n+3,n} &= \varsigma(\frac{(n+1)(n+2)(n+3)}{8})^{1/2}\omega\end{aligned}$$

leads to

$$\begin{aligned}\varepsilon_n &= (n+\frac{1}{2})\omega + \frac{15}{4}\varsigma^2(n+\frac{1}{2})^2\omega - ... \\ \Delta\varepsilon_n &= \varepsilon_n - \varepsilon_{n-1} \approx \omega(1 - \frac{15}{2}\varsigma^2 n)\end{aligned}$$

following [Kri06].

List of Figures

Bibliography

[ABB+98] A. Assion, T. Baumert, M. Bergt, T. Brixner, B. Kiefer, V. Seyfried, M. Strehle, and G. Gerber. Control of Chemical Reactions by Feedback-Optimized Phase-Shaped Femtosecond Laser Pulses. *Science*, 282:919, 1998.

[AdP02] P.W. Atkins and J. de Paula. Physical Chemistry. Oxford Univ. Press, 2002.

[AE75] L. Allen and J.H. Eberly. Optical Resonance in two level atoms. Whiley, 1975.

[AF05] P.W. Atkins and R.S. Friedman. Molecular Quantum Mechanics. Oxford Univ. Press, 2005.

[ALV02] L. Acardi, Y.G. Lu, and I. Volovich. Quantum Theory and its Stochastic Limit. Springer, 2002.

[Ban94] A.D. Bandrauk. Molecules in Laser Fields. Dekker, 1994.

[BB02] V. S. Batista and P. Brumer. Coherent Control in the Presence of Intrinsic Decoherence: Proton Transfer in Large Molecular Systems. *Phys. Rev. Lett.*, 89:143201, 2002.

[BDNG01] T. Brixner, N.H. Damrauer, P. Niklaus, and G. Gerber. Photoselective adaptive femtosecond quantum control in the liquid phase. *Nature*, 414:57–60, 2001.

[BEMG92] T. Baumert, V. Engel, C. Meier, and G. Gerber. High laser field effects in multiphoton ionization of Na_2. Experiment and quantum calculations. *Chem. Phys. Lett.*, 200(5), 1992.

[BGTG91] T. Baumert, M. Grosser, R. Thalweiser, and G. Gerber. Femtosecond Time-Resolved Molecular Multiphoton Ionization: The Na_2 System. *Phys. Rev. Lett.*, 67(27), 1991.

[BH54] M. Born and K. Huang. Dynamical theory of crystal lattices. Oxford Univ. Press,, 1954.

[BHP99] H.-P. Breuer, W. Huber, and F. Petruccione. Stochastic Wave-Function Method versus Density Matrix: a Numerical Comparison. *Phys. Rev. A*, 59(2), 1999.

[BJ03] B.H. Bransden and C.J. Joachain. Physics of Atoms and Molecules. Pearson Education Limited, 2003.

[BKT97] A. Bartana, R. Kosloff, and D.J. Tannor. Laser cooling of internal degrees of freedom II. *J. Chem. Phys.*, 106:1435–48, 1997.

[Blo46] F. Bloch. Nuclear Induction. *Phys. Rev.*, 70(7), 1946.

[Blu96] K. Blum. Density Matrix Theory and Applications. Plenum Press, 1996.

[BM58] G.E.P. Box and M.E. Muller. A Note on the Generation of Random Normal Deviates. *Annals of Mathematical Statistics*, 29(2), 1958.

[BO27] M. Born and J.R. Oppenheimer. Zur Quantentheorie der Molekeln. *Ann. Phys.*, 84(457), 1927.

[BR01] J.S. Briggs and J.M. Rost. On the Derivation of the Time-Dependent Equation of Schrödinger. *Foundation of Physics*, 31(4):693–712, 2001.

[BS86] P. Brumer and M. Shapiro. Control of unimolecular reactions using coherent light. *Chem. Phys. Lett.*, 126(6):541–6, 1986.

[BS92] P. Brumer and M. Shapiro. Laser Control of Molecular Processes. *Annu. Rev. Phys. Chem.*, 43:257–82, 1992.

[BS03a] P. Brumer and M. Shapiro. Coherent control of molecular dynamics. *Rep. Prog. Phys.*, 66:859–942, 2003.

[BS03b] P. Brumer and M. Shapiro. Principles of the quantum control of molecular processes. Wiley-Interscience, 2003.

[Car93] H. Carmichael. An Open System Approach to Quantum Optics. Springer, 1993.

[CC70] S. Chapman and T.G. Cowling. The mathematical theory of non-uniform gases. Cambridge University Press, 1970.

[CTDL91] C. Cohen-Tannoudji, B. Diu, and F. Laloë. Quantum Mechanics, Vol. I. Wiley, 1991.

[DCM92] J. Dalibard, Y. Castin, and K. Mølmer. Wave-function approach to dissipative processes in quantum optics. *Phys. Rev. Lett.*, 68:580–3, 1992.

[EMT09] V. Engel, C. Meier, and D.J. Tannor. Local control theory: recent applications to energy and particle transfer processes in molecules. *Adv. Chem. Phys.*, 141:29–101, 2009.

[FFjS82] M.D. Feit, J.A. Fleck jr., and A. Steiger. Solution of the Schrödinger Equation by a Spectral Method. *J. Comput. Phys.*, 47:412–433, 1982.

[FJ05] M. Frigo and S.G. Johnson. The Design and Implementation of FFTW3. *Proceedings of the IEEE*, 93:216, 2005.

[Gar09] C.W. Gardiner. Stochastic methods: a handbook for the natural and social sciences. Springer, 2009.

[GEE05] S. Gräfe, M. Erdmann, and V. Engel. Population transfer in the multiphoton excitation of molecules. *Phys. Rev. A*, 72(013404), 2005.

[GM85] G. Gerber and R. Möller. Optical-optical double resonance spectroscopy of high vibrational levels of the Na_2 $A^1\Sigma_u^+$ state in a molecular beam. *Chem. Phys. Lett.*, 113(6):546, 1985.

[GME05] S. Gräfe, C. Meier, and V. Engel. Instantaneous dynamics and quantum control fields: Principle and numerical applications. *J. Chem. Phys.*, 122(184103), 2005.

[Grä05] S. Gräfe. Laser-control of molecular dynamics. PhD thesis, Universität Würzburg, 2005.

[GZ00] C.W. Gardiner and P. Zoller. Quantum Noise. Springer, 2000.

[Hei25] W. Heisenberg. Über quantentheoretische Umdeutung kinematischer und mechanischer Beziehungen. *Zeitschrift für Physik*, 33:879–93, 1925.

[HJC95] Z. Haba, L. Jakobczyk, and W. Cegla. Stochasticity and Quantum Chaos. Springer, 1995.

[HWT85] J.P. Heritage, A.M. Weiner, and R.N. Thurston. Picosecond pulse shaping by spectral phase and amplitude manipulation. *Opt. Lett.*, 10(12):609–611, 1985.

[Kam97] N.G. van Kampen. Derivation of the Quantum Langevin Equation. *J. Mol. Liq.*, 71:97–105, 1997.

[Kam01] N.G. van Kampen. Stochastic processes in physics and chemistry. Elsevier, 2001.

[KBCV+09] I. Kalkman, C. Brand, T.-B. Chau Vu, W.L. Meerts, Y.N. Svartsov, O. Dopfer, X. Tong, K. Müller-Dethlefs, S. Grimme, and M. Schmitt. The structure of phenol-Ar_n (n=1,2) clusters in their S_0 and S_1 states. *J. Chem. Phys.*, 130(224303), 2009.

[KH78] P. Kusch and M.M. Hessel. An analysis of the $B^1\Pi_u - X^1\Sigma_g^+$ band system of Na_2. *J. Chem. Phys.*, 68:2591, 1978.

[KK83] R. Kosloff and D. Kosloff. A Fourier Method Solution for the Time Dependent Schrödinger Equation as a Tool in Molecular Dynamics. *J. Comput. Phys.*, 52(35), 1983.

[KME09] R. Kritzer, C. Meier, and V. Engel. Local control of population transfer in molecules under fluctuating perturbations. *Chem. Phys. Lett.*, 477:75–79, 2009.

[Kos88] R. Kosloff. Time-Dependent Quantum-Mechanical Methods for Molecular Dynamics. *J. Phys. Chem.*, 92:2087–2100, 1988.

[KRG+89] R. Kosloff, S.A. Rice, P. Gaspard, S. Tersigni, and D.J. Tannor. Wavepacket dancing: achieving chemical selectivity by shaping light pulses. *Chem. Phys.*, 139:201–220, 1989.

[KRH83] D.D. Konowalow, M.E. Rosenkrantz, and D.S. Hochhauser. Electronic Transition Dipole Moment Functions and Difference Potentials for Transitions among low-lying states of Li_2 and Na_2. *J. Mol. Spec.*, 99:321–38, 1983.

[Kri06] J. Krieger. Stoffzusammenfassung/Skript: Theoretische Quantenmechanik und Anwendungen. Lecture Notes, 2006.

[KTE86] R. Kosloff and H. Tal-Ezer. A direct relaxation method for calculating eigenfunctions and eigenvalues of the Schrödinger equation on a grid. *Chem. Phys. Lett.*, 127(3), 1986.

[Lin76] G. Lindblad. On the Generators of Quantum Dynamical Semigroups. *Comm. Math. Phys.*, 48:119–130, 1976.

[Loi73] W.H. Loisell. Quantum Statistical Properties of Radiation. Wiley, 1973.

[Mai60] T.H. Maiman. Stimulated optical radiation in ruby. *Nature*, 187(4736):493–494, 1960.

[Max62] J.C. Maxwell. On physical lines of force. *Philos. Mag.*, 4(25):161–175, 1862.

[MCD93] K. Mølmer, Y. Castin, and J. Dalibard. Monte Carlo wave-function method in quantum optics. *J. Opt. Soc. Am. B*, 10:524–538, 1993.

[ME07] P. Marquetand and V. Engel. Local control theory applied to molecular photoassociation. *J. Chem. Phys.*, 127(084115), 2007.

[Mil93] I.M. Mills. Quantities, units, and symbols in physical chemistry. Blackwell Scientific Publications, 1993.

[MM99a] E. Makarov and H. Metiu. Quantum dynamics with dissipation: A treatment of dephasing in the stochastic Schrödinger equation. *J. Chem. Phys.*, 111(22):10126–36, 1999.

[MM99b] E. Makarov and H. Metiu. Stochastic Schrödinger equation II: A study of the coherence seen in pump-probe experiments that use a strong pump laser. *J. Chem. Phys.*, 111(22):10137–47, 1999.

[MMT97] V.S. Malinovsky, C. Meier, and D.J. Tannor. Optical paralysis in electronically congested systems: application to large-amplitude vibrational motion of ground state Na_2. *Chem. Phys.*, 221:67–76, 1997.

[MS07] P. Meystre and M. Sargent. Elements of Quantum Optics. Springer, 2007.

[Muk95] S. Mukamel. Principals of Nonlinear Optical Spectroscopy. Oxford University Press, 1995.

[MW95] J. Manz and L. Wöste. Femtosecond Chemistry. VCH Weinheim, 1995.

[NRD94] K.A. Nelson, J.A. Rogers, and L.D. Dhar. Time-Resolved Vibrational Spectroscopy in the Impulsive Limit. *Chem. Rev.*, 94:157–193, 1994.

[Pau00] H. Pauly. Atom, Molecule and Cluster Beams, volume I,II. Springer, 2000.

[PDR88] A.P. Peirce, M.A. Dahleh, and H. Rabitz. Optimal control of quantum-mechanical systems: Existence, numerical approximation, and applications. *Phys. Rev. A*, 37(12), 1988.

[Pj07] C.P. Poole jr. The Physics Handbook: Fundamentals and Key Equations. Whiley VCH, 2007.

[PL66] P. Pechukas and J.C. Light. On the exponential form of time-displacement operators in Quantum Mechanics. *J. Chem. Phys.*, 44(10), 1966.

[PTVF92] W.H. Press, S.A. Teukolsky, W.T. Vetterlin, and B.P. Flannery. Numerical Recipes. Cambridge University Press, 1992.

[Red57] A.G. Redfield. The Theory of Relaxation Processes. *IBM Journal of Research and Development*, 1957.

[Rei02] K. Reich. Gauss' Werke in Kurzfassung. Rauner, 2002.

[Ris84] H. Risken. The Fokker Planck Equation. Springer, 1984.

[RZ00] S.A. Rice and M. Zhao. Optical control of molecular dynamics. Wiley, 2000.

[Saa96] P. Saalfrank. Stochastic wave packet vs. direct density matrix solution of Liouville-von Neumann

equations for photodesorption problems. *Chem. Phys.*, 211:265–276, 1996.

[SO96] A. Szabo and N.S. Ostlund. Modern Quantum Chemistry. Dover, 1996.

[SR07] K.P. Singh and J.M. Rost. Femtosecond photoionization of atoms under noise. *Phys. Rev. A*, 76(063403), 2007.

[SZ08] M.O. Scully and M.S. Zubairy. Quantum Optics. Cambridge University Press, 2008.

[Tan07] D.J. Tannor. Introduction to Quantum Mechanics. University Science Books, 2007.

[TJS83] A.J. Taylor, K.M. Jones, and A.L. Schawlow. Scanning pulsed-polarization spectrometer applied to Na_2. *J. Opt. Soc. Am. B*, 73:994, 1983.

[TKR86] D.J. Tannor, R. Kosloff, and S.A. Rice. Coherent pulse sequence induced control of selectivity of reactions: Exact quantum mechanical calculations. *J. Chem. Phys.*, 85:5805–20, 1986.

[Wei99] U. Weiss. Quantum Dissipative Systems. World Scientific, 1999.

[Wei00] A.M. Weiner. Femtosecond pulse shaping using spatial light modulators. *Rev. Sci. Instrum.*, 71:5, 2000.

[WKS+10] C. Walter, R. Kritzer, A. Schubert, C. Meier, O. Dopfer, and V. Engel. Dissipative Wave Packet Dynamics of Hydrophobic - Hydrophilic Site Switching in Phenol-Ar Clusters. *J. Phys. Chem. A*, 114:9743–9748, 2010.

[Wol97] B. Wolfseder. Modellrechnungen zur Dynamik und zeitaufgelösten Spektroskopie von ultraschnellen Elektron-Transfer Prozessen. PhD thesis, Technische Universität München, 1997.

[WRD93] W.S. Warren, H. Rabitz, and M. Dahleh. Coherent Control of Quantum Dynamics: The Dream is alive. *Science*, 259:1581–9, 1993.

[ZBD89] A.H. Zewail, R.M. Bowman, and M. Dantus. Femtochemistry of the Reaction: $IHgI^* \rightarrow [IHg \ ... \ I]^{\ddagger *} \rightarrow HgI + I$. *Chem. Phys. Lett.*, 156(2,3):131–137, 1989.

[ZMW87] P. Zoller, M. Marte, and D.F. Walls. Quantum jumps in atomic systems. *Phys. Rev. A*, 35(1):198, 1987.

Danksagung

Ganz herzlich möchte ich mich bei Prof. Dr. Volker Engel bedanken, dass er die Geduld aufwies, mich dieses Thema bearbeiten zu lassen. Auch möchte ich ihm für die Möglichkeit danken, mich auf Auslandsaufenthalten fortbilden zu können und stets auf offene Fragen bereitwillig einzugehen, vor allem als ein ausdauernder Lektor des vorliegenden Werkes.

Bei Prof. Dr. Christof Meier möchte ich mich für die Einblicke bedanken, die ich während meines Aufenthaltes in Toulouse gewinnen konnte. Für Hilfestellungen in meiner Einarbeitungsphase bin ich Dr. Philipp Marquetand und Dr. Joachim Seibt zu Dank verpflichtet. Im Laufe meiner Promotion erhielt ich ergiebige Unterstützung durch meine Kollegen Mirjam Falge, Klaus Renziehausen, Jost Henkel, Christoph Brüning, Kilian Hader, Christof Walter, Johannes Wehner, Anu Schaumlöffel, Martin Keß und in besonderem Maße von Alexander Schubert.

Des Weiteren spreche ich dem Arbeitskreis von Prof. Dr. Ingo Fischer sowie der gesamten PC und später dem AK Engels im IPTC meinen Dank für die nette Atmosphäre aus. Natürlich möchte ich mich bei meiner Familie für ihre Unterstützung bedanken und insbesondere bei meiner Verlobten, Carmen.